An improved hydro-biogeochemical model (CNMM-DNDC V6.0) for simulating dynamical forest-atmosphere exchanges of carbon and evapotranspiration at typical sites subject to subtropical and temperate monsoon climates in eastern Asia

Wei Zhang[1,2], Xunhua Zheng[1,2,3], Siqi Li[1], Shenghui Han[1], Chunyan Liu[1,3], Zhisheng Yao[1,3], Rui Wang[1], Kai Wang[1], Xiao Chen[1], Guirui Yu[4,5], Zhi Chen[4,5,6], Jiabing Wu[7], Huimin Wang[4], Junhua Yan[8], Yong Li[1]

[1] State Key Laboratory of Atmospheric Boundary Layer Physics and Atmospheric Chemistry, Institute of Atmospheric Physics, Chinese Academy of Sciences, Beijing 100029, P. R. China

[2] Qilu Zhongke Institute of Carbon Neutrality, Jinan 250100, China

[3] College of Earth and Planetary Sciences, University of Chinese Academy of Sciences, Beijing 100049, P. R. China

[4] Key Laboratory of Ecosystem Network Observation and Modeling, Institute of Geographic Sciences and Natural Resources Research, Chinese Academy of Sciences, Beijing 100101, China

[5] College of Resources and Environment, University of Chinese Academy of Sciences, Beijing 100049, China

[6] Beijing Yanshan Earth Critical Zone National Research Station, University of Chinese Academy of Sciences, Beijing 101408, China

[7] Institute of Applied Ecology, Chinese Academy of Sciences, Shenyang 110016, China

[8] South China Botanical Garden, Chinese Academy of Sciences, Guangzhou 510650, China

Correspondence to: Siqi Li (lisiqi@mail.iap.ac.cn); Yong Li (yli@mail.iap.ac.cn)

Abstract. Carbon exchange between forest ecosystems and the atmosphere play an important role in global carbon cycle, which is difficult to be accurately quantified due to the large uncertainties in scaling up site-scale observations or filling-up measurement gaps. A process-oriented model equipped with comprehensive processes to explicitly simulating coupled carbon, nitrogen and water cycling, is hypothesized to reduce the uncertainties in quantification of forest carbon fluxes. To test this hypothesis, the Catchment Nutrient Management Model - DeNitrification-DeComposition (CNMM-DNDC), as a hydro-biogeochemical model that dynamically couples the carbon, nitrogen, phosphorous and water cycling processes, was updated in this study by incorporating a new forest growth module derived from the Biome-BGC model and validating the updates using multiple-year continuous observations of carbon and water fluxes at the site scale. The updated model has

Geoscientific
Model Development
Discussions

29   improved the processes of photosynthesis, litter decomposition, allocation, respiration and mortality to more effectively

30   capture the transformation and transportation of nutrients in plant-soil-water continuum. The observed gross primary

31   productivity (GPP), ecosystem respiration (ER), net ecosystem carbon dioxide exchange (NEE) and evapotranspiration (ET)

32   of three typical forest sites subject to subtropical and temperate climates in eastern Asia (2003–2010) were used for the

33   model calibration and validation. Compared with the original model in validation, the updated model showed significant

34   improvements in simulating the daily dynamics and inter-annual variations of each variable, with the NRMSE values

35   decreased by 46% and 54%, 65% and 37%, 4% and −6%, and 38% and −3% for GPP, ER, NEE, and ET on daily and annual

36   scales, respectively. The comparable performances of both model versions for annual NEE emphasizes the importance of

37   validating each component of carbon fluxes to avoid the offsetting of model errors. The canopy average specific leaf area,

38   fraction of leaf nitrogen in Rubisco, annual leaf and fine root turnover fraction, maximum stomatal conductance and the ratio

39   of carbon to nitrogen in leaves and fine roots were identified as the sensitive eco-physiological parameters affecting the

40   simulations of GPP and ER. In addition, the meteorological variables of solar radiation, humidity and air temperature also

41   showed strong influences on the simulated GPP and ER. The relatively satisfactory performances demonstrated that the

42   modified model has the ability to capture the daily dynamics and inter-annual variations of carbon fluxes for forests in

43   temperate and subtropical zones, which is essential for estimating the emissions of greenhouse gases at the regional or global

44   scales.

45   **1 Introduction**

46   Forest ecosystems are widely spread in the world, which accounts for nearly 40% of the Earth's ice-free land surface

47   (Waring and Running, 1998). In spite of providing wood products, forests can also prevent soil erosion, maintain

48   biodiversity and regulate the water and carbon cycles (Waring and Running, 1998; Chiesi *et al.*, 2007). Forests play an

49   important role in global carbon cycle by regulating atmospheric carbon dioxide (CO_2) level via the photosynthesis. In

50   combating with climate change, forest can remove approximately one quarter of CO_2 emitted by combustion of fossil fuels

51   and industry through carbon sequestration (Seidl *et al.*, 2017; Cook-Patton *et al.*, 2020; FAO, 2020). Hence, accurate

52   estimation of forest carbon fluxes, such as gross primary productivity (GPP) and ecosystem respiration (ER), is essential for

53   understanding terrestrial ecosystem carbon cycle and stabilizing global climate change (Mao *et al.*, 2016; Ren *et al.*, 2022).

54   Various methods can be applied to estimate the carbon fluxes of forests, such as eddy-covariance techniques, satellite-based

55   remote sensing and numerical models. In comparison, the numerical models are promising tools to combine data from

56   different sources for more complete characterization of vegetation and soil processes. Among different types of numerical

57   models, including statistical/regression models (Tatarinov and Cienciala, 2006; Raj *et al.*, 2014), light use efficiency models

58   (Running *et al.*, 2004; Yuan *et al.*, 2014) and process-oriented models, the last type is essential scientific tools that, deal with

59   the atmosphere, vegetation, soil, and water within a given space as a continuous and dynamic system (Makela *et al.*, 2000;

60   Mao *et al.*, 2016). The process-oriented models are generally established based on theoretical understandings of

61   biogeochemical or even hydro-biogeochemical processes, and thus can better estimate the terrestrial carbon budget

62   influenced by multiple factors (Schulze *et al.*, 2009; Friedlingstein and Prentice, 2010; Hidy *et al.*, 2012).

63   Some process-oriented models have been developed to simulate carbon cycle of natural/undisturbed forest ecosystems

64   at regional or global scale, such as Biome-BGC, ORCHIDEE and LPJ (White *et al.*, 2000; Sitch *et al.*, 2003; Krinner *et al.*,

65   2005). As managed ecosystems are playing essential roles in terrestrial carbon budget, more researches have most recently

66   focused on the managed ecosystems with significant anthropogenic activities, such as afforested forests and croplands (Cai

67   *et al.*, 2022; Ciais *et al.*, 2013; Liu *et al.*, 2022; Mao *et al.*, 2016; Miyauchi *et al.*, 2019). Meanwhile, it is now clear that

68   interactions between climate and carbon cycle are affected by nitrogen availability and hydrology processes in ecosystems

69   (Thornton *et al.*, 2007; Piao *et al.*, 2013). The consideration of carbon-nitrogen interactions, as well as nutrients limitations

70   and availability and/or dynamics of water, in the process-oriented model substantially changes simulated dynamics of several

71   critical feedbacks between land and climate systems (e.g., Churkina *et al.*, 2009; Thomas *et al.*, 2013). Thus, the explicit

72   simulations of the nitrogen cycle and the interactions among carbon, nitrogen and water cycles have been improved in some

73   biogeochemical models. For instance, the widely applied Biome-BGC has been improved to create Biome-BGCMuSo by

74   adding a multilayer soil module, implementing the processes related to soil moisture and nitrogen balance, and incorporating

75   the vegetation managements suitable for managed forests and croplands (Thornton *et al.*, 2002; Bond-Lamberty *et al.*, 2005;

76   Tatarinov and Cienciala, 2006; Di Vittorio *et al.*, 2010; Hidy *et al.*, 2016). Other models suitable for undisturbed ecosystems

77   have also been extended to simulate the interactions of carbon, nitrogen and water in the managed ecosystems (e.g.,

78   croplands) with higher accuracy, such as ORCHIDEE-STICS and LPJmL (Gervois *et al.*, 2004; Bondeau *et al.*, 2007). For

79   croplands, some other process-oriented models have also been established to simulate the complex biogeochemical processes,

80   such as DNDC, WNMM, SPACSYS and WHCNS (Li *et al.*, 1992; Li, 2007; Wu *et al.*, 2007; Liang *et al.*, 2016). The

81   DNDC model has been extended to PnET-N-DNDC and Wetland-DNDC versions, which are suitable for forest and wetland

82   ecosystems (Li *et al.*, 2000; Zhang *et al.*, 2002). The WNMM model has been updated to the CNMM model by incorporating

83   the new hydrological module and improving plant growth module fitted for different types of vegetation (Ma *et al.*, 2018).

84   As the biogeochemical processes closely link with the hydrological processes, especially for the landscapes with undulating

85   terrain (e.g., catchments or river basins), hydro-biogeochemical models are believed to be more effective tools for studying

86   the carbon, nitrogen and water cycles for terrestrial ecosystems. Generally, hydro-biogeochemical models are based on

87   distributed or semi-distributed hydrological models and biogeochemical models with different levels of complexity, such as

88   LandscapeDNDC-CMF, SWAT-DayCent and CNMM-DNDC (Haas *et al.*, 2012; Wu *et al.*, 2016; Zhang *et al.*, 2018).

89   The CNMM-DNDC is a hydro-biogeochemical model. It was initially developed by fully coupling the Catchment

90   Nutrient Management Model (CNMM) and the DeNitrification-DeComposition Model (DNDC) and then further updated

91   several times to enable comprehensive simulations of the tightly coupled carbon, nitrogen, phosphorous and water cycles at

92   site, catchment, river basin, regional and even continental scales (Zhang et al., 2018; Zhang et al., 2018; Zhang et al., 2021a;

93   Zhang et al., 2021b; Li et al., 2022; Li et al., 2023). This model has been applied in different catchments located in various

94   climate regions by simultaneously simulating the ecosystem productivity, emissions of greenhouse gases and gaseous air

95   pollutants, and hydrological nitrogen losses through soil leaching and discharge in streams as well as soil erosion from an

96   entire catchment or individual landscape units (Zhang *et al.*, 2018; Zhang *et al.*, 2021a; Zhang *et al.*, 2021b; Li *et al.*, 2022; Li

97   *et al.*, 2023). At present, this model has been validated with multiple simultaneously variables, including crop yields, soil

98   organic carbon contents, emissions of methane, nitrous oxide, nitric oxide and ammonia, hydrological losses of nitrate and

99   total nitrogen through surface runoff and stream flows, and sediments production in soil erosion, in a subtropical agro-forest

100   catchment (Zhang *et al.*, 2018; Li *et al.*, 2023). The comprehensive validation demonstrated the strong capacity of the

101   CNMM-DNDC model in simulating the hydro-biogeochemical processes of terrestrial ecosystems.

102   Despite the sufficient validations in croplands, the model performance in simulating the forest ecosystems has not been

103   comprehensively evaluated due to limited data. It is very necessary to assess the model performance in the forest ecosystems

104   due to the vital role of forests in the terrestrial carbon budget (Seidl *et al.*, 2017). In addition, the present CNMM-DNDC

105   model simulates vegetation growth by adapting the module applied in the BIOME3 model, which sets the plants as an

106   entirety without biomass allocation among different tissues and/or organs. Such simplification may induce large

107   uncertainties, as both photosynthetic allocation and mortality are substantially important for accurately simulating the carbon

108   and nitrogen cycles of forest ecosystems. Therefore, we hypothesize that modification of the current vegetation growth

109   module by improving the simulation mechanisms of related processes, such as biomass allocation, respiration, and mortality,

110   can improve the performance of the CNMM-DNDC in simulating the carbon cycle of forest ecosystems in different climate

111   regions. To achieve such improvements is especially necessary to broaden the applicability and to increase the reliability of

112   this model.

113   To test the above hypothesis, the original and modified versions of the CNMM-DNDC model were evaluated for their

114   simulation of the daily GPP, ER, net ecosystem carbon dioxide exchange (NEE) and evapotranspiration (ET) using the

115   continuously observed multiple-year data of three typical forests subject to subtropical and temperate monsoon climates in

116   the eastern Asia. The overarching goals of this study are to (i) attempt to fill the gaps of simulation mechanisms in the

117   CNMM-DNDC model by improving the scientific processes of vegetation growth, (ii) compare the performances of the

118   original and modified model versions in simulating the GPP, ER, NEE and ET at the three typical forest sites and, (iii)

119   identify the eco-physiological parameters and model inputs that are sensitive to the simulated GPP and ER of the examined

120   forests. The new model version with the validated modifications is expected to be applicable for more accurately estimating

121   the carbon budget of forest ecosystems.

Geoscientific
Model Development
Discussions

2 Materials and methods

2.1 Model description

2.1.1 Overview of CNMM-DNDC

The initial version of the CNMM-DNDC model was established by incorporating the soil carbon and nitrogen transformation/transferring processes of the DNDC model, including the processes of decomposition, nitrification, denitrification and fermentation, into the distributed hydrological framework of the CNMM model (Zhang *et al.*, 2018). All other functions of the initial CNMM-DNDC version, such as those on the phosphorous cycle and vegetation growth, were directly inherited from the CNMM (Li *et al.*, 2017; Zhang *et al.*, 2018). Its later versions were established through several updates to improve its comprehensive functions and universally applicability. These updates include a) developing new soil pH regulation mechanisms for tea plantations (Zhang *et al.*, 2020), b) modifying the energy balance and heat conductivity mechanism for adaptation to freeze-thaw cycles in permafrost regions (Zhang *et al.*, 2021b), c) developing an alga-regulation mechanism of flooding water pH and introducing the Jayaweera-Mikkelsen mechanism for ammonia transfer between water and the atmosphere to improve the simulation of ammonia volatilization from paddy rice fields (Li *et al.*, 2022) and, d) introducing the ROSE mechanism on soil erosion to enable the simulations of hydraulic soil erosion and hydrological losses of dissolved and particle carbon, nitrogen and phosphorous components (Li *et al.*, 2023). As this model has been developed based on the basic theories of physics, chemistry, and biogeochemistry, it has realized systematic simulation of the tightly coupled carbon, nitrogen and water cycles at the catchment scale.

The simulated soil depth and temporal and spatial resolutions of the model are all allowed to user-defined depending on the availability of driving data and/or research objectives. The simulated soil profile could be down to 4 m deep. The soil temperature is calculated based on energy balance and heat conductivity. The soil moisture is simulated based on the mass balance among precipitation, irrigation, evapotranspiration, vertical flow, lateral flow and water from a rising groundwater table. For the site scale simulation, only surface runoff is taken into account, but the subsurface lateral flow is not. The infiltrated water is controlled by a defined maximum infiltration rate. The vertical water movement in the soil profile is calculated following the Darcy's law. A cell-by-cell approach using a kinematic approximation is applied to route the saturated

146 overland and subsurface flow based on the digital elevation model. A cascade of linear channel reservoirs is used for

147 calculating the stream flow (Wigmosta *et al.*, 1994). The soil biogeochemical processes are generally based on the first-order

148 kinetics for organic matter decomposition and the Michaelis-Menten kinetics of two substrates for nitrification and

149 denitrification while using the concept of an "anaerobic balloon" to allow for simultaneously oxidative and reductive

150 reactions (Li, 2007). For more details on the simulations of the soil biogeochemical processes, please see Li (2000, 2007), Li

151 *et al.* (2022, 2023) and Zhang *et al.* (2018, 2020, 2021).

152 In the current CNMM-DNDC model, the growth processes of plants, including crops, forests and grasslands, are adapted

153 from those applied in the BIOME3 model (Haxeltine and Prentice, 1996a, b). Among these processes, photosynthesis rate is

154 calculated as functions of absorbed photosynthetically active radiation (APAR), temperature and atmospheric CO_2

155 concentration, following Farquhar *et al.* (1980) for C_3 species and Collatz *et al.* (1992) for C_4. More explicitly, the net

156 photosynthesis rate, i.e., net primary productivity, is calculated using a standard nonrectangular hyperbola formulation, which

157 gives a gradual transition between two limiting rates describing the responses of photosynthesis to APAR and the Rubisco

158 abundance (Haxeltine and Prentice, 1996b). For more details on vegetation growth in the current CNMM-DNDC version,

159 please see Haxeltine and Prentice (1996a, b) and Zhang *et al.* (2018). The currently adopted simulation mechanisms on plant

160 growth, however, ignore not only the biomass allocation among different plant organs or tissues but also the processes of

161 mortality, even though both photosynthetic allocation and mortality are substantially important for accurately simulating the

162 carbon and nitrogen cycles of forest ecosystems.

2.1.2 Improvements of CNMM-DNDC

164 In this study, a new module of forest growth were established for the CNMM-DNDC model, by referring to the

165 simulation mechanisms applied in the Biome-Bio Geochemical Cycles (Biome-BGC) model (White *et al.*, 2000) to improve

166 the model performance in simulating the plant growth of forest ecosystems, as well as the related water and carbon fluxes. This

167 module is designed to well simulate the processes of photosynthesis, litter decomposition, photosynthetic allocation,

168 respiration and mortality of forests.

169   **2.1.2.1 Carbon pools of forest ecosystems**

170   Its carbon pools consist of plant carbon, coarse woody debris carbon, litter carbon and soil carbon. The plant carbon pool

171   is divided into sub-pools of leaves, fine roots, live stems, dead stems, live coarse roots and, dead coarse roots. The coarse

172   woody debris pool is the accepter of dead stems and dead coarse roots. The litter carbon pool is made of four constituents,

173   which are liable carbon, unshielded cellulose, shielded cellulose and, lignin. The soil carbon pool excluding the litter carbon is

174   initially inherited from the DNDC model, which includes the sub-pools of microbes, humads and humus.

175   **2.1.2.2 Photosynthesis**

176   The photosynthesis is one of the important individual processes for carbon accumulation in a forest ecosystem. The

177   photosynthesis rate is simulated separately for sun and shade leaves based on the two-leaf mechanism in consideration of

178   enzyme kinetics (Farquhar *et al.*, 1980). It jointly depends on the amount of APAR, the calculated maintenance respiration

179   (MR), the difference between the internal and external partial pressure of CO_2, the nitrogen content in leaves, the portion of

180   nitrogen in Rubisco and, the temperature controlling the enzyme kinetics.

181   The projected leaf area index of whole canopy ($PLAI_{total}$, in $m^2 \ m^{-2}$) is calculated as the product of average specific leaf

182   area based on carbon mass and leaf carbon content. The projected leaf area indexes for the sun leaves ($PLAI_{sun}$, $m^2 \ m^{-2}$) and

183   the shade leaves ($PLAI_{shade}$, $m^2 \ m^{-2}$) are calculated following Eqs. 1−2 (Jones, 1992).

$$PLAI_{sun} = 1 - e^{-PLAI_{total}} \qquad\qquad \text{Eq. 1}$$

$$PLAI_{shade} = PLAI_{total} - PLAI_{sun} \qquad\qquad \text{Eq. 2}$$

184   The amount of APAR ($APAR_{total}$, $APAR_{sun}$, $APAR_{shade}$, $W \ m^{-2}$) is calculated based on the incoming shortwave radiation

185   (Rads, in $W \ m^{-2}$), albedo (Alb, dimensionless), canopy light extinction coefficient (k, dimensionless), the $PLAI_{total}$ and, the

186   fraction of PAR in the incoming shortwave radiation (f_{par}, dimensionless) for the sun and shade leaves, respectively (Eqs. 3−5).

$$APAR_{total} = f_{par}Rads(1.0 - Alb)(1.0 - e^{-kPLAI_{total}}) \qquad\qquad \text{Eq. 3}$$

$$APAR_{sun} = f_{par}kPLAI_{sun}Rads(1.0 - Alb) \qquad\qquad \text{Eq. 4}$$

$$APAR_{shade} = APAR_{total} - APAR_{sun} \qquad\qquad \text{Eq. 5}$$

187   Three separate equations (Eqs. 6–8) are followed to calculate the reaction rate of photosynthesis, which is the process of

188   generating simple sugars by combining the CO_2 and H_2O molecules using energy from the sun (Farquhar *et al.*, 1980).

189   The Eq. 6 shows the regulation of CO_2 diffusion on the photosynthetic rate regulated by Rubisco (A_v, µmol CO_2 m^{-2} s^{-1})

190   or by electron transfer(A_j, µmol CO_2 m^{-2} s^{-1}), wherein C_a and C_i (Pa) are the atmospheric and intercellular concentrations of

191   CO_2, respectively. The C_a is calculated using Eq. 7, based on the input data of atmospheric pressure (pa, Pa) and CO_2

192   concentration (C_{co_2}, µmol mol^{-1}). Following Eq. 8 (Nobel, 1991), the stomatal conductance of CO_2 (g_{CO_2}, µmol m^{-2} s^{-1} Pa^{-1})

193   is calculated using the conductance of water vapour (g_{H_2O}, m s^{-1}), air temperature (T_{air}, °C), the universal gas constant ($R =$

194   8.3143，m^3 Pa mol^{-1} K^{-1}) and, the ratio of molecular weights of water vapour to CO_2 (M). The A_v or A_j in Eq. 6 is on the PLAI

195   basis.

$$A_{v\ or\ j} = g_{CO_2}(C_a - C_i) \qquad \text{Eq. 6}$$

$$C_a = 10^{-6} C_{co_2} pa \qquad \text{Eq. 7}$$

$$g_{CO_2} = \frac{10^6 g_{H_2O}}{MR(T_{air} + 273.15)} \qquad \text{Eq. 8}$$

196   The A_v is simulated by Eqs. 9–16. In Eq. 10, the maximum rate of carboxylation (V_{max}, µmol CO_2 m^{-2} s^{-1}) is simulated as

197   a function of the nitrogen mass in per unit area of sun or shade leaves (N_{leaf}, kg N m^{-2}), the fraction of leaf nitrogen in Rubisco

198   as an input parameter (f_{NR}, kg N kg^{-1} leaf N), the weight proportion of Rubisco relative to its nitrogen content (WP = 7.16, kg

199   Rub kg^{-1} Rubisco N) (Fasman, 1976) and the activity of Rubisco (AC, µmol CO_2 kg^{-1} Rub s^{-1}). Using Eq. 11, the nitrogen

200   concentration (N_{leaf}) in sun and shade leaves are calculated based on the input parameters of the mass ratio of carbon to

201   nitrogen (C:N) in leaves (r_{cnl}, dimensionless) and specific leaf area (SLA, m^2 kg^{-1} C). In Eq. 12, the AC is adapted by air

202   temperature (T_{air}, °C) from its standard value at 25 °C (AC_{25}, µmol CO_2 kg^{-1} Rub s^{-1}), wherein the AC_{25} value and the

203   temperature sensitivity coefficient (Q_{10AC}, dimensionless) are set as 6×10^4 µmol CO_2 kg^{-1} Rub s^{-1} and 2.4, respectively. The

204   compensation point of intercellular CO_2 concentrations (γ, Pa) in the absence of leaf maintenance respiration (MR_{leaf}, µmol

205   CO_2 m^{-2} s^{-1}) is a function of atmospheric concentration of oxygen gas (C_{O_2}, Pa) and the kinetic constants for Rubisco

206   carboxylation (K_c, Pa) and oxygenation (K_o, Pa) adapted by temperature (Eq. 13). The C_{O_2} is assumed to be 21% in the

207   atmosphere (Air, Pa) by volume (Eq. 14). The K_c and K_o values are adapted from their constants at the standard condition

208 (25 °C, $K_{c25} = 40.4$ Pa, and $K_{o25} = 24800$ Pa) to the T_{air} condition, using the Q_{10} values of 2.1 and 1.2, respectively, as the

209 temperature sensitivity coefficients for variables (Eqs. 15−16). The MR_{leaf} in Eq. 9 is on the PLAI basis (refer to the section of

210 2.1.2.5).

$$A_v = \frac{V_{max}(C_i - \gamma)}{C_i + K_c(1 + \frac{C_{O_2}}{K_o})} - MR_{leaf} \qquad \text{Eq. 9}$$

$$V_{max} = WPN_{leaf}f_{NR}AC \qquad \text{Eq. 10}$$

$$N_{leaf} = \frac{1}{r_{cnl}SLA} \qquad \text{Eq. 11}$$

$$AC = \begin{cases} \dfrac{1.8AC_{25}Q_{10AC}^{(\frac{T_{air}-15}{10})}}{Q_{10AC}} & T_{air} \leq 15\ °C \\ AC_{25}Q_{10AC}^{(\frac{T_{air}-25}{10})} & T_{air} > 15\ °C \end{cases} \qquad \text{Eq. 12}$$

$$\gamma = 0.5K_c\frac{C_{O_2}}{K_0} \qquad \text{Eq. 13}$$

$$C_{O_2} = 0.21Air \qquad \text{Eq. 14}$$

$$K_c = \begin{cases} \dfrac{1.8K_{c25}Q_{10K_c}^{(\frac{T_{air}-15}{10})}}{Q_{10K_c}} & T_{air} \leq 15\ °C \\ K_{c25}Q_{10K_c}^{(\frac{T_{air}-25}{10})} & T_{air} > 15\ °C \end{cases} \qquad \text{Eq. 15}$$

$$K_o = K_{o25}Q_{10K_o}^{(\frac{T_{air}-25}{10})} \qquad \text{Eq. 16}$$

211 The A_j is simulated by following Eqs. 17−20. Using the Eq. 18 (de Pury and Farquhar, 1997), the rate of electron

212 transport rate per unit leaf area (J, μmol CO_2 m^{-2} s^{-1}) is simulated as a function of potentially maximum rate of electron

213 transport rate per unit leaf area (J_{max}, μmol CO_2 m^{-2} s^{-1}), curvature of leaf response of electron transport to irradiance ($\theta_1 = 0.7$)

214 and PAR effectively absorbed by photosynthesis per unit leaf area (I_e, μmol CO_2 m^{-2} s^{-1}). The I_e is calculated by Eq. 19, based

215 on total absorbed PAR per unit leaf area (I, μmol CO_2 m^{-2} s^{-1}), spectral correction factor ($f_{sc} = 0.15$) and photons absorbed by

216 photosynthesis per transported electron (ppe, mol mol^{-1}). The I is a function of APAR and PLAI using the unit conversion

217 coefficient (EPAR) of 4.55 from W m^{-2} to μmol CO_2 m^{-2} s^{-1} for the sun and shade leaves (Eq. 20). The values of ppe are 2.6

218 and 3.5 for C_3 and C_4 plant, respectively.

$$A_j = \frac{J(C_i - \gamma)}{4.5 C_i + 10.5\gamma} - MR_{leaf} \qquad \text{Eq. 17}$$

$$\theta_1 J^2 - (I_e + J_{max})J + I_e J_{max} = 0 \qquad \text{Eq. 18}$$

$$I_e = I \frac{(1 - f_{sc})}{ppe} \qquad \text{Eq. 19}$$

$$I = EPAR \frac{APAR_{sun/shade}}{PLAI_{sun/shade}} \qquad \text{Eq. 20}$$

219   Equations 6 and 9 are solved for C_i, which in turn is introduced into Eq. 17 to solve A_j. The smaller value between the A_v

220   and A_j solutions is accepted as the rate of photosynthesis on the PLAI basis.

221   **2.1.2.3 Litter decomposition**

222   The carbon and nitrogen from dead leaves and fine roots are directly moved into four litter compartments according to the

223   specified proportions, while the nitrogen removed from the leaves before senescence is re-translocated. The turnover of live to

224   dead stems and coarse roots happens daily at a rate determined annually using the annual maximum live woody mass and the

225   specified live wood turnover rate. The dead stems and coarse roots are received by the coarse woody debris pool which is

226   fragmented and allocated to the litter pools. The litter pools then decompose and enter into the soil organic matter pools. The

227   decomposition of shielded cellulose, liable carbon, unshielded cellulose and lignin to unshielded cellulose, liable microbe,

228   liable humads and resistant humads, as well as the heterotrophic respiration and nitrogen immobilization by microbes during

229   these processes, are considered in the model, with the actual decomposition being scaled depending on the competing plant

230   nitrogen demand during allocation. Following Eq. 21 (White *et al.*, 2000), the potential nitrogen immobilization (N_{immo_p}, kg N

231   m^{-2} (3h)$^{-1}$) by microbial decomposition is calculated using the potential decomposed carbon (C_{decom_p}, kg C m^{-2} (3h)$^{-1}$),

232   fractions of heterotrophic respiration (f_{HR}, dimensionless) and C:N ratio of litter (R_{litCN}, dimensionless) and soil organic matter

233   (R_{soilCN}, dimensionless). The fractions related to the decomposition processes of leaf, fine root, stem and litters, as well as the

234   maximum rate constants and biomass loss through heterotrophic respiration, are all defined as constants (online supplementary

235   material of Table S1 and S3). The decomposition rates of litters are also adjusted by the soil temperature (t_adjust) and

236   moisture (w_adjust) as showed in Eq. 22−23, with the calculated soil water pressure under saturation and the minimum soil

237   water pressure ($Min_{pressure}$) set as −10 Mpa.

$$N_{\text{immo\_p}} = C_{\text{decom\_p}} \frac{1 - f_{\text{HR}} - \dfrac{R_{\text{litCN}}}{R_{\text{soilCN}}}}{R_{\text{soilCN}}} \qquad \text{Eq. 21}$$

$$t\_adjust = \begin{cases} e^{4.344692 - \frac{1}{(T_{\text{air}}+273.15) - 227.13}} & T_{\text{air}} \geq \text{-10 °C} \\ 0 & T_{\text{air}} < \text{-10 °C} \end{cases} \qquad \text{Eq. 22}$$

$$w\_adjust = \begin{cases} \dfrac{\ln(\dfrac{\text{Min}_{\text{pressure}}}{\text{SM}_{\text{pressure}}})}{\ln(\dfrac{\text{Min}_{\text{pressure}}}{\text{Sat}_{\text{pressure}}})} & \text{SM}_{\text{presssure}} > \text{Sat}_{\text{pressure}} \\ 1.0 & \text{SM}_{\text{presssure}} > \text{Sat}_{\text{pressure}} \\ 0.0 & \text{SM}_{\text{pressure}} < \text{Min}_{\text{pressure}} \end{cases} \qquad \text{Eq. 23}$$

2.1.2.4 Allocation

The assimilated carbon allocation and the nitrogen competition between plant nitrogen uptake and litter decomposition are calculated from the potential carbon quantity assimilated ($C_{\text{assi\_p}}$, kg C m^{-2} (3h)$^{-1}$) in photosynthesis and the potential microbial nitrogen demand ($N_{\text{immo\_p}}$, kg N m^{-2} 3h^{-1}) in organic matter decay.

The assimilated carbon ($C_{\text{assi\_p}}$, kg C m^{-2} (3h)$^{-1}$) available to allocate is the difference between gross primary productivity (GPP, kg C m^{-2} (3h)$^{-1}$) and MR (kg C m^{-2} (3h)$^{-1}$) of all live tissues. If the difference is negative, it means a carbon pool deficit; and thus the available carbon for allocation is first allocated to alleviate the deficit. All new allocations to other organs or tissues are constrained by the new leaf carbon allocation (Waring and Running, 2007). The carbon required for per unit of leaf growth ($C_{\text{allometry}}$, dimensionless), which is the carbon allometry, is calculated based on the fractions of user-defined allocation rates and growth respiration (f_{GR}, dimensionless), which in turn accounts for 30% of the total carbon in new tissue (Eq. 24). The key allocation ratios include new fine root carbon to new leaf carbon (r_{frtol}, dimensionless), new stem carbon to new leaf carbon (r_{stol}, dimensionless), new live wood carbon to new total wood carbon (r_{lwtow}, dimensionless) and new coarse root carbon to new stem carbon (r_{crtos}, dimensionless). According to Eq. 25, the associated nitrogen needed by per unit of leaf growth ($N_{\text{allometry}}$, dimensionless), which is the nitrogen allometry, is calculated based on carbon allometry and the C:N ratios of leaf (R_{lCN}, dimensionless), fine root (R_{frCN}, dimensionless), live wood (R_{lwCN}, dimensionless) and dead wood (R_{dwCN}, dimensionless) (Eq. 25). The nitrogen demand for plant growth ($N_{\text{assi\_p}}$, kg N m^{-2} (3h)$^{-1}$) is predicted by the potential

Geoscientific
Model Development
Discussions

254   assimilated carbon ($C_{\text{assi\_p}}$, kg C m^{-2} (3h)$^{-1}$), carbon allometry ($C_{\text{allometry}}$, dimensionless) and nitrogen allometry ($N_{\text{allometry}}$,

255   dimensionless), using Eq. 26. The total nitrogen demand (N_{demand}, kg N m^{-2} (3h)$^{-1}$) is the sum of the potential nitrogen

256   immobilization ($N_{\text{immo\_p}}$, kg N m^{-2} (3h)$^{-1}$) and the nitrogen demand for plant growth ($N_{\text{assi\_p}}$, kg N m^{-2} (3h)$^{-1}$).

$$C_{\text{allometry}} = (1 + f_{\text{GR}})[1 + r_{\text{frtol}} + r_{\text{stol}}(1 + r_{\text{crtos}})] \qquad \text{Eq. 24}$$

$$N_{\text{allometry}} = \frac{1}{R_{\text{lCN}}} + \frac{r_{\text{frtol}}}{R_{\text{frCN}}} + \frac{r_{\text{stol}} r_{\text{lwtow}}(1 + r_{\text{crtos}})}{R_{\text{lwCN}}} + \frac{r_{\text{stol}}(1 - r_{\text{lwtow}})(1 + r_{\text{crtos}})}{R_{\text{dwCN}}} \qquad \text{Eq. 25}$$

$$N_{\text{assi\_p}} = C_{\text{assi\_p}} \frac{N_{\text{allometry}}}{C_{\text{allometry}}} \qquad \text{Eq. 26}$$

257   If the soil available mineral nitrogen (N_{soil}, kg N m^{-2} (3h)$^{-1}$) can satisfy the total nitrogen demand, the actual allocation

258   and microbial decomposition are equal to the potential values. The plant nitrogen demand is first addressed by the

259   retranslocated nitrogen and then the soil mineral nitrogen. The nitrogen demand for decomposition is totally from the soil

260   mineral nitrogen. Otherwise, the potential microbial decomposition is adjusted by a dimensionless factor of FPI, which is

261   defined with N_{soil} and the ratio $N_{\text{immo\_p}}$ to N_{demand} (Eq. 27). The N_{demand} is still provided by the retranslocated nitrogen and soil

262   mineral nitrogen pools. If the N_{demand} can be satisfied by the nitrogen pools, the actual nitrogen allocations are equal to the

263   potential nitrogen allocations. Otherwise, the actual nitrogen allocations are proportionally reduced (Wang *et al.*, 2009).

$$\text{FPI} = \frac{N_{\text{soil}} \dfrac{N_{\text{immo\_p}}}{N_{\text{demand}}}}{N_{\text{immo\_p}}} \qquad \text{Eq. 27}$$

264   **2.1.2.5 Respiration**

265   The maintenance respiration (MR, kg C m^{-2} (3h)$^{-1}$) is a function of the nitrogen concentration of living plant tissues (N,

266   kg N m^{-2}), temperature sensitivity ($Q_{10} = 2.0$) and T_{air} (Eq. 28). The plant nitrogen concentration is assumed to linearly affect

267   MR, with a relationship of 0.218 kg C d^{-1} kg^{-1} N (Ryan, 1991). The MR is separately calculated for leaves, fine roots, live

268   stems and live coarse roots. The leaf maintenance respiration (MR$_{\text{leaf}}$, μmol CO$_2$ m^{-2} s^{-1}) on the PLAI basis is separately

269   calculated for sun and shade leaves, based on the nitrogen concentration on the PLAI basis (N_{leaf}, kg N m^{-2}), Q_{10}, T_{air} and the

270   molar mass of carbon ($M_{\text{CO}_2} = 12$ g mol^{-1}) (Eq. 29).

Geoscientific
Model Development
Discussions
EGU
Open Access

$$\text{MR} = \frac{0.218 N Q_{10}^{\frac{T_{\text{air}}-20}{10}}}{8} \qquad \text{Eq. 28}$$

$$\text{MR}_{\text{leaf}} = \frac{0.218 N_{\text{leaf}} Q_{10}^{\frac{T_{\text{air}}-20}{10}}}{86400 \times 10^{-9} M_{\text{CO}_2}} \qquad \text{Eq. 29}$$

271   The growth respiration (GR, kg C m^{-2} (3h)$^{-1}$) is calculated separately for plant organs of leaves, fine roots, live stems, and

272   live coarse roots. For a plant organ, its GR is calculated by allocating the carbon in this organ to its GR pool. The stored GR

273   pool of this organ is fully or partly converted to the growth in the next year using two key parameters. One is the fraction of

274   carbon respired for growth ($g_1 = 0.3$). And the other is the proportion of growth respiration to release at fixation ($g_2 = 1.0$). The

275   carbon pools of plant organs are calculated in the allocation module.

2.1.2.6 Mortality

276

277   The mortality is calculated for all plant organs using user-defined rates and the dead tissues enter the pools of coarse

278   woody debris and litters at each time step. In addition, plant mortality due to fire can be simulated using a user specified rate,

279   which results in the losses of carbon and nitrogen to the atmosphere.

2.2 Description of observed data

280

281   The observed data for model validation were obtained from the Chinese Terrestrial Ecosystem Flux Observation and

282   Research Network (ChinaFLUX) which was established in 2002 (http://www.chinaflux.org/enn/index.aspx). Using the

283   open-path eddy covariance techniques, continuous measurements of carbon and water fluxes have been conducted since then

284   in the major typical forest ecosystems of the eastern Asia, including the temperate site (42 °24′09″N, 128 °05′45″E, 738 m a.s.l.)

285   in Changbai Mountain (CBM) with mixed forest of evergreen needle leaf and deciduous broad leaf trees, The subtropical site

286   (26 °44′29″N, 115 °03′29″E, 102 m a.s.l.) at Qianyanzhou (QYZ) with artificial evergreen coniferous forest and the subtropical

287   site (23 °10′25″N, 112 °32′04″E, 300 m a.s.l.) in the Dinghu Mountain (DHM) with evergreen mixed forests of broad and

288   needle leaf trees (Yu *et al.*, 2008; Yu *et al.*, 2013; Zhang *et al.*, 2019a). All the forests at the three sites have been treated as

289   natural reservation area without management. The available datasets for the model calibration and validation at the three sites

290 included daily GPP, ER, NEE and ET measured in 2003 to 2010. Meanwhile, the observed hourly meteorological datasets,

291 including air temperature, precipitation, radiation, wind speed and relative humidity, were used as model inputs to drive the

292 simulation.

293 The CBM forest site is located in northeast China and situated within the National Natural Conversation Park of the

294 Changbai Mountains, in the eastern Jilin Province (Guan *et al.*, 2006). The region is subjected to a temperate continental

295 monsoon climate, with an average annual air temperature of 3.6 °C and annual precipitation of 695 mm (1985−2005) (Yu *et al.*,

296 2008). A homogeneous mixture of broad leaf deciduous and evergreen coniferous (red pine) forest widely distributes in the

297 natural reservation area (Wu *et al.*, 2021).

298 The QYZ site is located in southeast China and situated the Jiangxi Province. The region is subjected to a subtropical

299 continental monsoon climate, with mean annual air temperature of 17.9°C and annual precipitation of 1475 mm (1985−2007)

300 (Wen *et al.*, 2010). The artificial pure coniferous forests were established in 1985 (Dai *et al.*, 2021).

301 The DHM site is located in south China and situated in the Dinghu Mountains Biosphere Reserve of the Guangdong

302 Province. The region is subjected to a typical subtropical monsoon humid climate, with an average annual air temperature of

303 22.3 °C and annual precipitation of 1678 mm, of which 80% falls between April and September (Zhou *et al.*, 2013). The carbon

304 and water fluxes were observed in a mixed forest of evergreen broad leaf and conifer trees, which is a major forest type in

305 low-latitude subtropical eastern Asia (Li *et al.*, 2012).

306 More detailed site descriptions can be referred to the online supplementary material of Table S2.

307 **2.3 Model simulation**

308 The modified CNMM-DNDC was calibrated and validated using the observed data of carbon and water fluxes from 2003

309 to 2007 and 2008 to 2010, respectively, in each of the three forest sites. The required input data of climate (T_{air}, precipitation

310 (Prec), wind speed (Wind), solar radiation (Rad), and relative humidity (Hum) in the resolution of 3-hour) and basic soil

311 properties (soil clay fraction, organic matter content (SOM), total nitrogen, pH and bulk density (BD)) were primarily

312 obtained from the National Ecosystem Science Data Center (NESDC; http://www.cnern.org.cn). The climate data out of the

313 observational period were obtained from the China meteorological forcing dataset (1979–2018) (https://data.tpdc.ac.cn).

314   Additional required soil parameters also as model inputs, including field capacity, wilting point and saturated hydrological

315   conductivity, were calculated using pedo-transfer functions (Li *et al.*, 2019). The mixed forests were assumed as

316   homogeneously distributed deciduous broad leaf tree (DBT) and evergreen needle leaf tree (ENT) for the CBM and

317   evergreen broad leaf tree (EBT) and evergreen needle leaf tree (ENT) for the DHM. The vegetation type at the QYZ site was

318   a pure ENT. The required parameters for forest simulation, including forest type, carbon contents of leaf and stem and

319   eco-physiological parameters (Table S3), were primarily adapted from the field observations provided by the NESDC or

320   from the peer reviewed literatures (Zeng *et al.*, 2008; Li, 2018; Li, 2019). The simulated soil profile (0−1.5 m in depth) was

321   divided into 16 layers, with layer thicknesses of 0.05, 0.1 and 0.5 cm for the 0–0.5, 0.5–1 and 1–1.5 m depths, respectively.

322   In order to stabilize the carbon and nitrogen dynamics and thus reduce the residual effects of initial conditions (Zhang *et al.*,

323   2015), especially for the carbon balance among different pools, which requires spin-up for at least 10 years (Palosuo *et al.*,

324   2012), the model simulation at each forest site was pre-run for 13 years.

2.4 Sensitivity analysis

326   The one-at-a-time (OAT) sensitivity analysis was adopted to examine the influences of newly involved parameters in

327   the modified CNMM-DNDC model and the inputs as primary drivers on the simulated GPP and ER from the investigated

328   forest ecosystems. As the NEE was the difference between ER and GPP, it was not considered in the sensitivity analysis.

329   The simulations during the validation periods (2008–2010) for the three forest sites were regarded as the baseline. The

330   eco-physiological parameters required for the newly established forest growth module were involved in the sensitivity

331   analysis, which are detailed in Table S3. In each OAT sensitivity analysis of parameters, a parameter was altered by $\pm 20\%$,

332    $\pm 15\%$ and $\pm 10\%$, with the others remaining constant (White *et al.*, 2000). In addition, meteorological variables (i.e., T_{air},

333   Rad, Wind and Hum as 3-hourly means and Prec as 3-hourly totals during the validation periods) and soil properties (i.e.,

334   soil clay fraction, pH, SOM content and BD) were involved in the sensitivity analysis of model inputs. In the OAT

335   sensitivity analysis of model inputs, the values of a meteorological variable during the validation periods and the value of a

336   soil property were altered by $\pm 20\%$, $\pm 15\%$ and $\pm 10\%$, but with exception for T_{air}, BD and pH; while the other

337   meteorological inputs remained unaltered and the other soil properties remained constant. The 3-hourly average of T_{air} during

338   the validation period was altered within the range of –3 to +3 $^{\circ}$C with an interval of 1 $^{\circ}$C. Considering that real soil BD and

339   pH usually vary with narrow amplitudes, the former property was altered within the ranges of 0.97 to 1.17 (CBM), 1.20 to

340   1.40 (QYZ) and 1.28 to 1.48 (DHM), with an interval of 0.04, and the latter within the ranges of 4.64 to 5.64 (CBM), 4.1 to

341   4.9 (QYZ) and 3.3 to 4.3 (DHM), with an interval of 0.2, respectively. The sensitivity of annual GPP and ER fluxes to an

342   examined parameter or input variables was evaluated using a sensitivity index (I, %) following Majkowski $et\ al.$ (1981).

343   Each I value was calculated with Eq. 30.

$$I = \frac{100 \sum_{i=1}^{n} (|M_i - M_{\text{baseline}}|)}{n M_{\text{baseline}}} \qquad \text{Eq. 30}$$

344   In Eq. 30, M_i and M_{baseline} denote the simulated annul GPP or ER corresponding to the ith altered value(s) and the

345   baseline of the examined parameter or input variables, respectively; and n represents the total number of alternation for a

346   parameter or input variable, which was set as 6 in this study. The three-year mean and standard deviation of a forest type at

347   each site were reported for the value of index (I), indicating the sensitivity of annual GPP or ER fluxes to a parameter or an

348   input variable.

349   **2.5 Statistics and analysis**

350   The statistical criteria applied for evaluating the model performance in this study (Eqs. 31−33) included (i) the

351   normalized root mean square error (NRMSE), (ii) the Nash–Sutcliffe efficiency (NSE), and (iii) the determination coefficient

352   (R^2) and slope of a significant linear zero-intercept regression (ZIR) (Nash and Sutcliffe, 1970; Willmott and Matsuurra, 2005;

353   Moriasi $et\ al.$, 2007; Congreves $et\ al.$, 2016; Dubache $et\ al.$, 2019). A value of NRMSE closer to 0 indicated a better simulation.

354   The NSE value (ranging from minus infinity to 1) is defined to compare the overall deviation of the simulations from the

355   observations with the observed variance (Nash and Sutcliffe, 1970). An NSE of 1 indicates the best simulation, and a value

356   between 0 and 1 shows smaller overall deviation than the observed variance and thus an acceptable model performance, but

357   otherwise worse. A better model performance is also indicated by a slope and an R^2 value simultaneously closer to 1 in a

358   significant zero-intercept linear regression of observations against simulations (Dubache $et\ al.$, 2019). The absolute

359   divergence of the slope from 1 represents the average bias of the simulations from the observations (Zhang $et\ al.$, 2019b).

$$\text{NRMSE} = \frac{1}{|\bar{O}|}\sqrt{\frac{\sum_{i=1}^{n}(S_i-O_i)^2}{n}} \qquad \text{Eq. 31}$$

$$\text{NSE} = 1 - \frac{\sum_{i=1}^{n}(S_i-O_i)^2}{\sum_{i=1}^{n}(O_i-\bar{O})^2} \qquad \text{Eq. 32}$$

$$R^2 = 1 - \frac{\sum_{i=1}^{n}(O_i-\hat{O}_i)^2}{\sum_{i=1}^{n}(O_i-\bar{O})^2} \qquad \text{Eq. 33}$$

In Eqs. 31−33, i and n (i = 1, 2, …, n) denote the ith pair and the total number of pairs of the model simulated (S), observed (O) and predicted ($\hat{O}$) by linear regression, respectively, with the n values given in Tables 1−2 and $\bar{O}$ denoting the mean value of n observations.

In addition, the Taylor diagram was also used to evaluate the performances of the original and modified model versions. A Taylor diagram for all the three field sites was drawn for one of the four examined variables, i.e., GPP, ER, NEE and ET. It was used to simultaneously demonstrate the correlation coefficients (r) between the simulations and observations of daily fluxes, the centred root mean square difference (RMSD) and the standard deviations (SD) of the observations (the horizontal axis) and the model simulations. A normalized SD (NSD) of observations was 1 and the corresponding NSD of simulations was given as the ratio of the standard deviation of simulations to that of observations. A Taylor diagram would indicate a better model performance with r closer to 1 and a distance closer to zero between the RMSD of simulations and the NSD of observations.

The SPSS Statistics Client 19.0 (SPSS Inc., Chicago, USA), the Origin 8.0 (OriginLab, Northampton, MA, USA) and the R software packages were applied for the statistical analysis and graphical comparison. The source code and executive program of the improved model, as well as the input data can be obtained from Zhang *et al*. (2024).

3 Results

3.1 Model performances in simulating carbon and water fluxes

The daily GPP observed at the three forest sites all showed significant seasonal variation trends, which were consistent with the dynamics of air temperature. However, the seasonal patterns at the DHM site that is located in the south margin of subtropical region were much weaker than those at the other two sites. For the daily GPP simulations, as compared to the observations, the original model generally resulted in much earlier appearance of the seasonal peak at the CBM site (Fig. 1a),

380   larger inter-day fluctuations at the QYZ site and larger seasonal peak fluxes at the CBM and DHM sites (Figs. 1a, 2a and 3a).

381   The modified model overcome these poor performances of the original model, with the NRMSE, NSE and R^2 and slope

382   values of 0.33−0.41, 0.08−0.89, 0.18−0.90, and 0.85−0.94 respectively (Figs. 1a, 2a and 3a; Table 1). At each site, the

383   modified model generally performed better than the original model, as showed in the Taylor diagram (Fig. 4a). Among the

384   three sites, the modified model showed the best performance at the CBM site, with NSE (~0.88), R^2 (~0.89) and slope

385   (~0.94), all beings close to 1. In comparison, especially at the CBM and DHM sites, the daily GPP fluxes simulated by the

386   original model were much higher than the observations during the growing season, which led to the unacceptable statistics

387   (Table 1). The observed annual GPP fluxes during the eight years ranged from 13.3 to 16.6, 16.5 to 19.3 and 12.5 to 15.5 Mg

388   C ha^{-1} yr^{-1} at the CBM, QYZ and DHM, respectively. The corresponding annual simulations by the original versus modified

389   models totalled 12.4−18.5 versus 14.5−18.3, 14.4−19.2 versus 17.6−20.3, and 12.8−14.0 versus 12.7−15.2 Mg C ha^{-1} yr^{-1},

390   respectively (Fig. 5a−c), with the modified model resulted in an NSE over 0.60. Thus, the modified model showed better

391   performances in simulating the annual GPP fluxes than the original model (Table 2). The validation results of GPP showed

392   that the modified model not only performed much better in simulating the daily dynamics during multiple years, but also

393   more effectively captured the inter-annual variations.

394   The daily observed ER showed similar dynamics with those of GPP, but the peak values at the CBM sites were nearly

395   double of those at the DHM site. For the daily ER fluxes, the original model resulted in earlier appearance of the seasonal

396   peaks at the CBM site, overestimated seasonal fluxes at the CBM and DHM sites and larger inter-day fluctuations or even

397   underestimation in summer at the QYZ site. In comparison, the modified model could successfully overcome these poor

398   performances (Figs. 1b, 2b and 3b). It could generally well capture the seasonal patterns, with much smaller deviations,

399   reporting the NRMSE, NSE, R^2 and slope values of 0.18−0.27, 0.62−0.93, 0.68−0.93 and 0.92−1.05, respectively, during

400   both the calibration and validation periods (Table 1). In contrast, the original model performed poorly in simulating the daily

401   ER fluxes of the three sites during both periods, showing NRMSE, NSE and R^2 ranged from 0.51 to 0.94, −1.32 to 0.25, 0.11

402   to 0.40 and 0.45 to 0.83, respectively (Table 1). The Taylor diagram also indicates the obvious improvements of ER

403   simulations by the modified model for the three forest sites, with significant higher correlation coefficients (Fig. 4b). For the

404   annual ER fluxes at the CBM, QYZ and DHM sites, the observations varied from 11.3 to 14.7, 12.1 to 15.7 and 9.0 to 11.4

405   Mg C ha^{-1} yr^{-1}, respectively. The corresponding simulations by the original versus modified models totalled 10.8−14.9

406   versus 11.1−16.2, 9.9−13.0 versus 12.7−14.3, and 9.5−10.3 versus 9.5−11.1 Mg C ha^{-1} yr^{-1}, respectively (Fig. 5d−f). The

407   simulations by the modified model were much better than the original model, showing NSE values of 0.56 versus 0.05 for all

408   cases (Table 2). These results on the model performances indicate that the modified model version developed in this study is

409   capable of well simulating the sum of CO_2 effluxes due to autotrophic respiration and soil heterotrophic respiration in

410   different forest types subject to subtropical to temperate monsoon climates in east Asia.

411   The observed daily NEE showed significant seasonal patterns at the CBM site, while less obvious seasonal patterns at

412   the other two sites (Figs. 1c, 2c and 3c). The Taylor diagram (Fig. 4c) illustrates that the modified model better simulated the

413   daily NEE fluxes of the CBM during either the calibration or validation period but not at the QYZ and DHM sites (Table 1),

414   as compared to the original model. However, the corresponding statistics for the NEE validation, with values of 1.05 to 2.85,

415   −0.11 to 0.47, 0.02 to 0.61 and 0.15−0.41 for the NRMSE, NSE, R^2 and slope, respectively, were generally worsen than

416   those for the GPP and ER (Table 1). The simulations by the original model did not match with the observations due to the

417   deviations in capturing the seasonal dynamics of GPP and ER. At the CBM site, especially, the original model resulted in

418   unreasonably intensive negative NEE in the spring season while the modified model in generally performed pretty good for

419   the dynamical daily NEE fluxes of this site (Fig. 1c). At the QYZ site, both model versions showed comparable

420   performances in simulating the daily NEE fluxes, though the modified model obviously improved its performances in

421   simulating the dynamical daily fluxes of both GPP and ER (Fig. 2c). At the DHM site, the simulations by both model

422   versions showed significant disagreement with the measured daily NEE fluxes in the winter season and occasionally also in

423   the summer season, though the modified model greatly improved the simulations of daily GPP and ER fluxes (Fig. 3c). The

424   annually accumulated NEE fluxes observed at the CBM, QYZ and DHM sites in 2003−2010 ranged from −3.8 to −0.7, −5.5

425   to −3.6 and −5.2 to −2.1 Mg C ha^{-1} yr^{-1}, respectively. The annual NEE fluxes simulated by the original versus modified

426   models ranged from −3.6 to −1.4 versus −4.2 to −1.8, −6.1 to −4.6 versus −6.8 to −3.9, and −3.0 to −3.7 versus −4.1 to −3.3

427   Mg C ha^{-1} yr^{-1} at the CBM, QYZ, and DHM sites, respectively (Fig. 5g−i). Despite the worse simulations of GPP and ER by

428   the original model, the simulated annual NEE fluxes were comparable between the two model versions (Table 2).

429   Overall, for the carbon fluxes of the three forest sites during the multiple-year periods, the modified model effectively

430   captured the dynamical GPP and ER, followed by the NEE (Fig. 1−3). For the different forest types, the modified model

431   better predict the annual NEE of the pure ENT (QYZ) and the mixing forest of ENT and DBT (CBM) than the mixing forest

432   of ENT and EBT (DHM) (Table 2). Following the definition of NEE (i.e. NEE = ER – GPP), the NRMSE of simulated daily

433   and annual NEEs could be propagated from those of GPP and ER simulations. For the daily NEEs during the validation

434   period, the propagated NRMSE values were 0.49, 0.40 and 0.42 at the CBM, QZY and DHM, respectively (0.44 on average

435   across the three sites). For the annual NEEs, the propagated NRMSE value across all the three sites during the three

436   validation years was 0.13. These propagated NRMSEs for the modified model simulations, as Table 1 and 2 list, were much

437   smaller than the NRMSEs of direct NEE simulations (0.44 versus 1.92 on average for the daily fluxes and 0.13 versus 0.51

438   for the annual fluxes), or as compared to the NRMSEs propagated from those of the original model simulations on ER and

439   GPP (0.44 versus 1.02 on average and 0.13 versus 0.23 for the daily and annual NEE fluxes, respectively).

440   The seasonal dynamics of daily ET fluxes were consistent with those of daily GPP due to the contribution of

441   transpiration which is closely related with plant growth. At the CBM sites, both model versions showed comparable good

442   performance in simulating the dynamical ET fluxes. At the other two sites, the original model failed to capture the seasonal

443   dynamics of ET fluxes, but the modified model performed as good as it did at the CBM site (Figs, 1d, 2d and 3d). The

444   modified model showed NRMSE, NSE, R^2 and slope values of 0.32−0.46, 0.59−0.81, 0.49−0.82 and 0.61−0.77 for

445   simulating the daily ET fluxes during the three-year validation period, respectively, especially with great improvement of

446   NSE (0.80 versus 0.00 at QYZ, and 0.59 versus −0.55 at DHM) as compared to the original model (Table 1). The Taylor

447   diagram also suggested that ET simulations by the modified model were significantly better at the sites of QYZ and DHM,

448   as compared to the original model (Fig. 4d). The observed annual ET quantities in 2000−2008 varied from 392 to 495, 510 to

449   768 and 574 to 720 mm at the CBM, QYZ and DHM sites, respectively. The annual ET simulated by the original versus

450   modified model versions amounted 332−485 versus 394−522, 696−800 versus 654−732, and 583−726 versus 614−725 mm

451   at the CBM, QYZ and DHM, respectively (Fig. 5j−l). In comparison, the modified model better captured the inter-annual

452   variations of ET, with an NSE value greater than 0.60 (Table 2). In general, the modified model with the updated plant

453   growth module performed better in not only in simulating the daily ET dynamics, but also the inter-annual variations.

454   In comparison with the original model, according to the statistics of daily validation fluxes for all the examined

455   variables including ($n = 12$) and excluding ($n = 9$) the NEE of all the three sites (Table 1), the modified model on average

456   reduced the NRMSE by 38% ($p < 0.01$) and 50% ($p < 0.01$), increased the NSE from −0.26 to 0.54 and −0.34 to 0.68,

457   enlarged the R^2 by 85% (from 0.39 to 0.72, $p < 0.05$) and 90% (from 0.42 to 0.80, $p < 0.05$), and reduced the absolutely

458   deviations of the slopes from 1 (from 0.35 to 0.12, $p < 0.01$ and from 0.33 to 0.04, $p < 0.001$), respectively. These results

459   further showed the obviously improved performances of the modified model in simulating daily fluxes of GPP, ER and ET,

460   particularly reduced significantly the biases of daily GPP and ER.

461   For the statistics of NRMSE, NSE, slope and R^2 on the annual GPP and ER at the three sites in the validation years, the

462   modified model showed slightly significant improvement ($n = 8$, $p < 0.01$), while those on the annual NEE and ET were

463   comparable between the modified and original model (Table 2).

464   **3.2 Sensitivity of carbon fluxes to examined parameters or factors**

465   For the newly incorporated eco-physiological parameters, as Figs 6−7 and Figs S1−2 illustrate, the modified model

466   simulations of both annually cumulated GPP and ER fluxes at the three sites were sensitive to canopy average specific leaf

467   area (SLA, p30), fraction of leaf nitrogen in Rubisco (FLNR, p32), annual fraction of leaf and fine root turnover (LFRT, p6)

468   and maximum stomatal conductance ($g_{CO_{2max}}$, p33). FLNR, LFRT and SLA were the parameter with the highest sensitivity

469   for the mixed forests at the CBM, QYZ and DHM sites, respectively. Both annual GPP and ER fluxes of the mixed forests at

470   the CBM and DHM sites were more sensitive to the parameter of FLNR than those of ENT at the QYZ site. Compared with

471   the forests in the temperate region, the annual GPP and Re fluxes of subtropical forests were more sensitive to the parameter

472   of LFRT. The values of sensitivity index were increased with the decreased latitude. For annually cumulated GPP fluxes,

473   SLA was the parameter with higher sensitivity for the ENT in different climate zones, while FLNR was the most sensitive

474   parameter for the DBT in the temperate region and the EBT in the subtropical region (Figs S1). The sensitivity index of

475   FLNR for the DBT was nearly twice of that for the ENT at the CBM site, and thus FLNR was identified as the most

476   sensitive parameter for the annual GPP fluxes at the CBM site. Similarly, the relatively high index of LFRT for the ENT at

477   the DHM site led to intensive responses of the simulated annual GPP fluxes to the changes of LFRT. With regard to the

478   sensitive parameters of annual ER fluxes, there were SLA, fine roots (C:N$_{fr}$, p17), LFRT and g_{smax} for the ENT and, FLNR,

479   LFRT and carbon to nitrogen ratios in leaves (C:N$_{leaf}$, p15) for the DBT and EBT (Figs S2).

480   For the meteorological variables, Figs. 6−7 demonstrate that the simulated annual GPP and ER fluxes were sensitive to

481   solar radiation and air temperature at the CBM and DHM sites with mixed forests, while were solar radiation and humidity at

482   the QYZ site. The values of sensitivity index were comparable among three sites. For the ENT, the annual GPP fluxes were

483   most sensitive to the solar radiation and humidity at the three sites in different climate zones. For the DBT and EBT, the

484   annual GPP and ER fluxes were most sensitive to the solar radiation and air temperature (Figs. S1−2). Meanwhile, both the

485   annual GPP and ER fluxes of the different forests were not sensitive to the examined soil properties of clay fraction, soil

486   organic matter, pH and bulk density with sensitivity indexes less than 1%.

487   **4 Discussions**

488   **4.1 Model simulations on carbon fluxes**

489   As GPP is an essential flux component in the carbon budget of forests at site to global scales, accurate estimation of

490   forest GPP is urgently required to understand and assess the dynamics of global carbon cycle, predict future trends and

491   ensure long term security of the ecosystem services (Campbell *et al.*, 2017; Cook-Patton *et al.*, 2020). Light use efficiency

492   (LUE) models, such as CASA, MODIS, can adequately simulate the spatial and temporal dynamics of GPP due to the usage

493   of extensive satellite observations (Potter *et al.*, 1993; Running *et al.*, 2004). By comparing and assessing major algorithms

494   and performances of seven LUE models, Yuan *et al.* (2014) have concluded that most models can effectively capture the

495   temporal variations and magnitudes of daily GPP in deciduous broad leaf forests and mixed forests (with R^2 of 0.6 to 0.8).

496   However, this type of model cannot be applied for prediction due to the dependence on satellite data that are only available

497   historically (Yuan *et al.*, 2014). As Raczka *et al.* (2013) have indicated, reproducing the inter-annual variability of GPP is a

498   challenge for both LUE and terrestrial biosphere models. Process-oriented models are designed to enable prediction of future

499   carbon cycle through describing the physical and mechanistic processes occurring over time (Srinet *et al.*, 2023). The

500   comparison studies of model simulation against the observations in North American (Keenan *et al.*, 2012; Raczka *et al.*,

501   2013) have showed that, as compared to LUE models, process-oriented models possess some skills in simulating the

502   inter-annual variations (with R of 0.09 to 0.46). In the present study, the modified process-oriented model well simulated the

503   multiple-year dynamics of daily GPP fluxes (with R^2 of 0.5 to 0.9) and showed acceptable performance in simulating

504   inter-annual GPP variations (with R^2 of 0.8). These results are comparable with or even better than the simulations of the

505   Biome-BGC model for the three forest sites involved in our study (Wen, 2019; Fan, 2021). The worst performance for the

506   forest at the DHM site may be attributed to the errors in simulating the photosynthesis of EBT due to the difficulty in

507   modelling the subtle changes in the leaf phenology. Such a difficulty has also been encountered by previous studies (Raczka

508   *et al.*, 2013; Yuan *et al.*, 2014). In addition, previous study has showed that assimilating satellite data, e.g., LAI, can

509   significantly improve the performance of process-oriented models in simulating daily GPP (Yan *et al.*, 2016). Therefore, for

510   the large scale studies, assimilating satellite data may provide a solution to further improve the ability of the modified

511   CNMM-DNDC model for simulating the spatial and temporal dynamics of forest GPP.

512   An ER flux consists of the flux components of plant autotrophic respiration and soil heterotrophic respiration, which is

513   derived from the organic carbon of all organisms in an ecosystem (Chapin et al., 2012). The uncertainties of ER simulations

514   can lead to the bias of other variables in carbon cycle, such as NEE and net primary production (Fang *et al.*, 2022). Lu *et al.*,

515   (2021) have found that terrestrial ecosystem models result in large divergences in simulating annual soil respiration and its

516   components (with R^2 less than 0.5). In this study, our modified model well simulated the multiple-year ER at the three sites,

517   with R^2 around 0.6 which was comparable with simulations based on the random forest model (Lu *et al.*, 2021). In addition,

518   compared with the ER at the DHM site, the intensive fluxes in the growing season at the CBM were primarily attributed to

519   the latitudinal gradients of temperature and precipitation along the North-South Transect in Eastern China (Yu *et al.*, 2008).

520   Field experiments observed highly spatial variability in Q_{10} as a temperature sensitivity parameter of ER, which is usually a

521   key parameter in the process-oriented models (Yu *et al.*, 2008; Anav *et al.*, 2013). However, inadequately considering the

522   spatial heterogeneity of Q_{10} in process-oriented models may lead to divergences in simulating ER. Therefore, mechanistic

523   parameterization of Q_{10} to better reflect the spatial heterogeneity of this parameter is still needed for large scale applications

524   of our modified model to estimate the carbon budgets of terrestrial ecosystems.

525   As compared to GPP and ER, the modified model performed worse in simulating NEE at either the daily or annual

526   scale. The highest uncertainty in predicting NEE is consistent with other studies, which may be due to the compounding

527   effects of GPP and ER errors (Fang *et al.*, 2022). Using the default and calibrated parameters or the assimilated satellite LAI

528   data, Liu (2018) have evaluated the performances of the Biome-BGC model in simulating the daily NEE of three years at the

529   three forest sites involved in our study and resulted in RMSEs of 9.3 to 31.6 kg C ha^{-1} d^{-1}. Our results during the validation

530   periods ranged from 14.6 to 16.9 kg C ha^{-1} d^{-1}, which were comparable to the results using the calibrated parameters in the

531   above study. At the annual scale, the correlation between simulated and observed GPP is consistently higher than that of

532   NEE, indicating the high sensitivity of NEE to small relative errors in large GPP fluxes (Raczka *et al.*, 2013). Meanwhile,

533   the correlation of ER between simulations and observations was lower than that of GPP, suggesting that ER may be the main

534   contributor to the poor simulation of inter-annual variability in NEE. Although process-oriented models can effectively

535   simulate the different types of carbon fluxes by incorporating the inter-annual influences of temperature and soil moisture,

536   the simulated NEE in this study, as well as others (Keenan *et al.*, 2012; Raczka *et al.*, 2013), can draw a conclusion that

537   process-oriented models do not adequately explain the observed inter-annual variability in NEE, yet. In addition, despite the

538   much better performances of our modified model in simulating both the daily and annual GPP and ER, the statistics of

539   simulated NEE were almost the same between the original and the modified model versions. These results suggest the

540   necessity of validating each component of carbon fluxes from ecosystems so as to avoid the offsetting of model errors.

541   **4.2 Sensitivity analysis**

542   As plant autotrophic respiration consumes nearly 50% of the carbon available from photosynthesis, ER is closely tied to

543   plant productivity, and thus the strong positive correlation between GPP and ER is presented in models (Ryan, 1991; Piao *et*

544   *al.*, 2013; Jagermeyr *et al.*, 2014). The analysis results of this study also indicated that the sensitive parameters of ER were

545   generally consistent with those of GPP. The parameters that were most sensitive for GPP and ER were those controlling the

546   CO_2 assimilation rate in photosynthesis and influencing respiration, such as SLA, FLNR, LFNR, $g_{CO_{2max}}$, C:N$_{leaf}$ and C:N$_{fr}$.

547   This result is consistent with those reported by White *et al.* (2000), Raj *et al.* (2014), Miyauchi *et al.* (2019), Ren *et al.* (2022)

548   and Srinet *et al.* (2023). Specific leaf area was identified as a sensitive parameter for both GPP and ER at the three sites as

549   the ENT were sensitive to SLA at all sites (Fig. S1). This parameter is widely used in process-oriented models for calculating

550   LAI which influences all aspects of canopy physiology (White *et al.*, 2000). Miyauchi *et al.* (2019) have concluded that SLA

551 strongly affects aboveground woody and leaf carbon density in *Eucommia ulmoides* plantations on the Loess Plateau.

552 Therefore, it is not surprising that the variations in SLA result in significant corresponding changes in GPP, as well as ER

553 (Srinet *et al.*, 2023). Our results also showed that both GPP and ER were sensitive to the parameter of FLNR, especially for

554 the broad leaf trees. Carboxylation is the first step of atmospheric CO_2 assimilation, using the catalyst of Rubisco which is

555 probably the most abundant protein on earth (Stitt and Schulze, 1994; White *et al.*, 2000). The fraction of leaf nitrogen in

556 Rubisco controls the potential rate of carboxylation (V_{max}). This potential rate is a significant state variable with high spatial

557 variability that is difficult to obtain (Houborg *et al.*, 2012). Thus, the intensive impacts of FLNR on GPP and ER are

558 reasonable (Raj *et al.*, 2014). In addition, LFRT was identified as a sensitive parameter for the forests in the subtropical

559 regions. For deciduous trees, all the leaf and fine root carbon pools are fully turned over every year and thus LFRT is set as

560 1.0. For evergreen trees, however, LFRT is given as the inverse of mean leaf longevity (White *et al.*, 2000). Net

561 photosynthetic capacity has been found to be negatively related with leaf longevity (Reich *et al.*, 1999). It is determined by

562 the positive relationship between LFRT and FLNR in our model. Due to the regulating effects of stomatal conductance on

563 water loss and carbon assimilation (White *et al.*, 2000; Miyauchi *et al.*, 2019), $g_{CO_{2max}}$ was recognized in our study as a

564 relatively sensitive parameter. In process-oriented models, e.g., the modified CNMM-DNDC, $C:N_{leaf}$ determines the nitrogen

565 required for leaf construction and the content of chlorophyll, thereby affecting photosynthesis, leaf respiration and net

566 primary cumulative productivity (White *et al.*, 2000; Ren *et al.*, 2022). Although $C:N_{fr}$ has no direct influences on the

567 uptakes of water and nutrients, it can control the nitrogen required for fine root construction and the allocation of nitrogen to

568 roots and shoots, and hence the corresponding respirations (Raj *et al.*, 2014). These may explain why $C:N_{leaf}$ and $C:N_{fr}$

569 showed relatively high sensitivity for the DBT and the ENT in the temperate region, respectively. The analysis of

570 eco-physiological parameters also suggests that the parameters of SLA, FLNR, LFNR and $g_{CO_{2max}}$ may be consistently

571 influential, independent of sites or the type of sensitivity analysis. But the ranking of the parameters may vary according to

572 specific species and regions (Raj *et al.*, 2014).

573 In the sensitivity analysis, solar radiation, air temperature and humidity were identified as the essential meteorological

574 variables influencing GPP. Solar radiation determines the rate of photosynthesis which depends on the amount of absorbed

575 photosynthetically active radiation. Theoretically, increased solar radiation can promote photosynthesis by providing more

576 photosynthetic photon (Yu *et al.*, 2008). As radiation change is the most pronounced factor during cloudy conditions, in

577 which leaves are not saturated with light, unlike in full-sunny conditions (Yu *et al.*, 2008), our analysis showed that a

578 positive change in solar radiation during cloudy conditions could significantly promote vegetation growth. The simulations

579 of the BEPS and CLM-CN models showed that increased solar radiation resulted in higher GPP (Raczka *et al.*, 2013), which

580 was consistent with the simulations of our modified CNMM-DNDC model. Air temperature was identified as the secondly

581 sensitive meteorological variable as it influence the enzymatic activity of photosynthesis for mixed forests in both CBM and

582 DHM with broadleaved trees (Farquhar *et al.*, 1980). Previous studies have showed that ER is closely tied to temperature and

583 plant productivity (Yu *et al.*, 2008; Jagermeyr *et al.*, 2014). Similar effect of temperature on ER was also detected in the

584 sensitivity analysis of this study. Air temperature and solar radiation can substantially affect the ER by regulating enzymatic

585 activity and plant growth. Apart from the effects of solar radiation and air temperature, those of humidity were remarkable

586 for the ENT, as increased humidity caused declined vapour pressure deficit and promoted leaf-scale conductance, thus

587 resulting in higher GPP and lower ET (Sato *et al.*, 2015). In addition, the limited effects of soil properties on GPP and ER

588 suggest that the variations of GPP and ER among the three field sites could be primarily attributed to the latitudinal gradients

589 of meteorological variables, e.g., air temperature.

590 The sensitively analysis can quantify the contribution of input parameters/variables to the changes in model outputs,

591 which is widely applied in model calibration, diagnostic evaluation and uncertainty assessment (Pianosi *et al.*, 2016). In this

592 study, the one-at-a-time approach of sensitivity analysis was used to evaluate the influences of newly introduced

593 eco-physiological parameters and model inputs on the GPP and ER fluxes simulated by the modified CNMM-DNDC.

594 However, the one-at-a-time approach has two essential limitations. One is that only the effects of a specific parameter/input

595 variable can be provided, but those of the other parameters/inputs cannot be examined during each simulation. Another is

596 that the analysis may be invalid when investigated output variable is non-linearly tied with an investigated parameter/input

597 variable (Saltelli *et al.*, 2008). A global approach of sensitivity analysis can reflect the interactive effects of changes in

598 multiple parameters/inputs (Saltelli et al., 2000; Odongo *et al.*, 2013; Raj *et al.*, 2014). Thus, in order to identify the most

599 influential input parameters and provide insight into the model function, global sensitivity analysis is needed in future study

600 to comprehensively analyse the effects of multiple inputs, such as the variance-based sensitivity analysis.

5 Conclusions

601

602   The Catchment Nutrient Management Model - DeNitrification-DeComposition (CNMM-DNDC) is a lately developed

603 process-oriented hydro-biogeochemical model. Its development is aiming at comprehensive simulation/prediction of

604 multiple ecosystem variables (e.g., emissions/uptakes of carbon and/or nitrogen gases from terrestrial ecosystems,

605 evapotranspiration, productivity, soil erosion, and slope runoff and catchment discharges of particle and/or dissolved carbon,

606 nitrogen and phosphorous at plot, ecosystem, landscape, catchment/river basin, regional or global scales), which are often

607 concerned in implementing the United Nations Sustainable Development Goals (SDGs) by 2030. However, the current

608 version of this model uses the same simulation mechanism of plant growth for forest, grassland, wetland and cropland

609 vegetation, thus resulting in large biases in simulating dynamical carbon fluxes of forests. In fact, the growth and turn over

610 processes of forests are often different from other vegetation types. In this study, by referring to the Biome-BGC model, the

611 current CNMM-DNDC model was updated through developing a special module on forest growth so as to improve its

612 simulation mechanisms of forest vegetation. The modified processes of the updated model include photosynthesis, allocation,

613 respiration, mortality and litter decomposition, which can detail the transformation and transportation of carbon and nitrogen

614 in the plant-soil-water continuum of forests. Using the daily data observed by the eddy covariance systems at three typical

615 forest sites located in different climate regions of the eastern Asia, the updated CNMM-DNDC model were calibrated and

616 validated for simulating the gross primary productivity (GPP), ecosystem respiration (ER), net ecosystem carbon dioxide

617 exchange (NEE) and evapotranspiration (ET) during the 8-years period of 2003–2010. The model can effectively reproduce

618 the daily dynamics of the carbon and water fluxes, thus showing a strong capacity in capturing their annual variations.

619 Compared with the original CNMM-DNDC, the updated model version generally performed much better in simulating the

620 daily GPP, ER and ET fluxes, but had no remarkable improvement for the daily NEE. This comparison suggests the

621 necessity of calibrating and validating each component of carbon fluxes to avoid the offsetting of model errors. The GPP and

622 ER fluxes simulated by the updated model version are remarkable sensitive to the changes in canopy average specific leaf

623 area, fraction of leaf nitrogen in Rubisco, annual leaf and fine root turnover fraction, maximum stomatal conductance and

624 ratios of carbon to nitrogen in leaves and fine roots as the eco-physiological parameters and solar radiation, humidity and air

625 temperature as the essential meteorological variables that regulate forest growth. However, the effects of soil properties on

the simulated GPP and ER were neglectable. The updated model was proven in this study to be capable of estimating the carbon fluxes of various forest ecosystems. It thus provides a potential tool for quantifying multiple ecosystem variables in close association with the SGDs, especially with improved credibility in simulating the carbon fluxes and budgets of forests. However, the robust performances of the modified CNMM-DNDC in comprehensively simulating the aforementioned ecosystem variables for addressing multiple SDGs at different scales still need verification and confirmation in further studies.

Code and data availability

The source code and executive program of the improved model, as well as the input data can be obtained from https://doi.org/10.5281/zenodo.13363688. All the observed data sets used in this study are available at the ChinaFLUX (http://nesdc.org.cn/).

Author contribution

Zhang, W., Li, S., Li, Y. and Zheng, X. contributed to the idea and science of this study. Zhang, W. programmed the newly developed module on forest growth, implemented the model simulations and data analysis and prepared the manuscript with contributions from all co-authors. Han, S. collected and established the input database for modelling. Yu, G., Chen, Z., Wu, J., Wang, H. and Yan, J. contributed to observation and quality assurance/quality control of the measured data involved in the updated model calibration and validation. Li, C., Yao, Z., Wang, R., Wang, K. and Chen, X. contributed to the manuscript improvement.

Competing interests

The authors declare that they have no conflict of interest.

Acknowledgement

Geoscientific
Model Development
Discussions

648   the National Key Scientific and Technological Infrastructure project "Earth System Science Numerical Simulator Facility"

649   (EarthLab).

References

651   Anav, A., Friedlingstein, P., Kidston, M., Bopp, L., Ciais, P., Cox, P., Jones, C., Jung, M., Myneni, R., Zhu, Z., 2013.
652   Evaluating the Land and Ocean Components of the Global Carbon Cycle in the CMIP5 Earth System Models. J. Climate
653   26, 6801–6843.

654   Bond-Lamberty, B., Gower, S.T., Ahl, D.E., Thornton, P.E., 2005. Reimplementation of the Biome-BGC model to simulate
655   successional change. Tree Physiol. 25, 413–424.

656   Bondeau, A., Smith, P.C., Zaehle, S., Schaphoff, S., Lucht, W., Cramer, W., Gerten, D., Lotze-Campen, H., MÜLler, C.,
657   Reichstein, M., Smith, B., 2007. Modelling the role of agriculture for the 20th century global terrestrial carbon balance.
658   Global Change Biol. 13, 679–706.

659   Cai, Z., Yan, X., Gu, B., 2022. Applying C:N ratio to assess the rationality of estimates of carbon sequestration in terrestrial
660   ecosystems and nitrogen budgets. Carbon Res. 1, 2.

661   Campbell, J.E., Berry, J.A., Seibt, U., Smith, S.J., Montzka, S.A., Launois, T., Belviso, S., Bopp, L., Laine, M., 2017. Large
662   historical growth in global terrestrial gross primary production. Nature 544, 84–87.

663   Chiesi, M., Maselli, F., Moriondo, M., Fibbi, L., Bindi, M., Running, S.W., 2007. Application of BIOME-BGC to simulate
664   Mediterranean forest processes. Ecol. Model. 206, 179–190.

665   Ciais, P., Sabine, C., Bala, G., Bopp, L., Brovkin, V., Canadell, J., Chhabra, A., DeFries, R., Galloway, J., Heimann, M.,
666   Jones, C., Le Quéré, C., Myneni, R. B., Piao S., and Thornton, P.: Carbon and Other Biogeochemical Cycles, in:
667   Climate Change 2013: The Physical Science Basis. Contribution of Working Group I to the Fifth Assessment Report of
668   the Intergovernmental Panel on Climate Change edited by: Stocker, T. F., Qin, D., Plattner, G. K., Tignor, M., Allen, S.
669   K., Boschung, J., Nauels, A., Xia, Y., Bex, V., and Midgley, P. M., 2013. Cambridge University Press, Cambridge,
670   United Kingdom and New York, NY, USA.

671   Chapin, F.S., Matson, P.A., Vitousek, P.M. 2012. Principles of terrestrial ecosystem ecology.

672   Churkina, G., Brovkin, V., von Bloh, W., Trusilova, K., Jung, M., Dentener, F., 2009. Synergy of rising nitrogen depositions
673   and atmospheric CO_2 on land carbon uptake moderately offsets global warming. Global Biogeochem. Cy. 23, GB4027.

674   Collatz, G.J., Ribas-Carbo, M., Berry, J.A., 1992. Coupled photosynthesis-stomatal conductance model for leaves of C_4
675   plants. Aust. J. Plant Physiol. 19, 519–538.

676   Congreves, K.A., Dutta, B., Grant, B.B., Smith, W.N., Desjardins, R.L., Wagner-Riddle, C., 2016. How does climate
677   variability influence nitrogen loss in temperate agroecosystems under contrasting management systems? Agr. Ecosyst.
678   Environ. 227, 33–41.

679   Cook-Patton, S.C., Leavitt, S.M., Gibbs, D., Harris, N.L., Lister, K., Anderson-Teixeira, K.J., Briggs, R.D., Chazdon, R.L.,
680   Crowther, T.W., Ellis, P.W., Griscom, H.P., Herrmann, V., Holl, K.D., Houghton, R.A., Larrosa, C., Lomax, G., Lucas,
681   R., Madsen, P., Malhi, Y., Paquette, A., Parker, J.D., Paul, K., Routh, D., Roxburgh, S., Saatchi, S., van den Hoogen, J.,

682   Walker, W.S., Wheeler, C.E., Wood, S.A., Xu, L., Griscom, B.W., 2020. Mapping carbon accumulation potential from
683   global natural forest regrowth. Nature 585, 545–550.

684   Dai, X., Wang, H., , X., Mingjie, Yang, F., Wen, X., Chen, Z., Zhang, L., Sun, X., Yu, G., 2021. An observation dataset of
685   carbon and water fluxes of artificial coniferous forests in Qianyanzhou (2003–2010). China Sci. Data 6, 2020-2006-2002.

686   de Pury, D.G.G., Farquhar, G.D., 1997. Simple scaling of photosynthesis from leaves to canopies without the errors of big-leaf
687   models. Plant Cell Environ. 20, 537–557.

688   Di Vittorio, A.V., Anderson, R.S., White, J.D., Miller, N.L., Running, S.W., 2010. Development and optimization of an
689   Agro-BGC ecosystem model for C4 perennial grasses. Ecol. Model. 221, 2038–2053.

690   Dubache, G., Li, S., Zheng, X., Zhang, W., Deng, J., 2019. Modeling ammonia volatilization following urea application to
691   winter cereal fields in the United Kingdom by improving a biogeochemical model. Sci. Total Environ. 660, 1403–1418.

692   Fan, H., 2021. Simulation and analysis of water use efficiency in three terrestrial ecosystems. Dissertation, Northwest A & F
693   University.

694   Fang, J., Shugart, H.H., Liu, F., Yan, X., Song, Y., Lv, F., 2022. FORCCHN V2.0: an individual-based model for predicting
695   multiscale forest carbon dynamics. Geosci. Model Dev. 15, 6863–6872.

696   FAO, 2020. Global Forest Resources Assessment 2020. FAO.

697   Farquhar, G., Caemmerer, S., Berry, J., 1980. A biochemical model of photosynthetic CO_2 assimilation in leaves of C_3 species.
698   Planta 149, 78–90.

699   Fasman, G.D., 1976. Handbook of Biochemistry and Molecular Biology. Proteins, III. Cleveland, OH, CRC Press.

700   Friedlingstein, P., Prentice, I.C., 2010. Carbon–climate feedbacks: a review of model and observation based estimates. Curr.
701   Opin. Env. Sust. 2, 251–257.

702   Gervois, S., de Noblet-Ducoudré, N., Viovy, N., Ciais, P., Brisson, N., Seguin, B., Perrier, A., 2004. Including croplands in a
703   global biosphere model: methodology and evaluation at specific sites. Earth Interact. 8, 1–25.

704   Guan, D., Wu, J., Zhao, X., Han, S., Yu, G., Sun, X., Jin, C.J., 2006. CO_2 fluxes over an old, temperate mixed forest in
705   northeastern China. Agr. Forest Meteorol. 137, 138–149.

706   Haas, E., Klatt, S., Fröhlich, A., Kraft, P., Werner, C., Kiese, R., Grote, R., Breuer, L., Butterbach-Bahl, K., 2012.
707   LandscapeDNDC: a process model for simulation of biosphere–atmosphere–hydrosphere exchange processes at site and
708   regional scale. Landscape Ecol. 28, 615–636.

709   Haxeltine, A., Prentice, I.C., 1996a. BIOME3: An equilibrium terrestrial biosphere model based on ecophysiological
710   constraints, resource availability, and competition among plant functional types. Global Biogeochem. Cy. 10, 693–709.

711   Haxeltine, A., Prentice, I.C., 1996b. A general model for the light-use efficiency of primary production. Brit. Ecol. Soc. 10,
712   551–561.

713   Hidy, D., Barcza, Z., Haszpra, L., Churkina, G., Pintér, K., Nagy, Z., 2012. Development of the Biome-BGC model for
714   simulation of managed herbaceous ecosystems. Ecol. Model. 226, 99–119.

715   Hidy, D., Barcza, Z., Marjanović, H., Ostrogović Sever, M.Z., Dobor, L., Gelybó, G., Fodor, N., Pintér, K., Churkina, G.,
716   Running, S., Thornton, P., Bellocchi, G., Haszpra, L., Horváth, F., Suyker, A., Nagy, Z., 2016. Terrestrial ecosystem
717   process model Biome-BGCMuSo v4.0: summary of improvements and new modeling possibilities. Geosci. Model Dev. 9,
718   4405–4437.

719 Houborg, R., Cescatti, A., Migliavacca, M., 2012. Constraining model simulations of GPP using satellite retrieved leaf
720   chlorophyll. In: IEEE International Geoscience and Remote Sensing Symposium (IGARSS). pp. 6455–6458.

721 Jagermeyr, J., Gerten, D., Lucht, W., Hostert, P., Migliavacca, M., Nemani, R., 2014. A high-resolution approach to estimating
722   ecosystem respiration at continental scales using operational satellite data. Global Change Biol. 20, 1191–1210.

723 Jones, H.G., 1992. Plants and Microclimate. Cambridge, Cambridge University Press.

724 Keenan, T.F., Baker, I., Barr, A., Ciais, P., Davis, K., Dietze, M., Dragoni, D., Gough, C.M., Grant, R., Hollinger, D., Hufkens,
725   K., Poulter, B., McCaughey, H., Raczka, B., Ryu, Y., Schaefer, K., Tian, H., Verbeeck, H., Zhao, M., Richardson, A.D.,
726   2012. Terrestrial biosphere model performance for inter-annual variability of land-atmosphere CO_2 exchange. Global
727   Change Biol. 18, 1971–1987.

728 Krinner, G., Viovy, N., de Noblet-Ducoudré, N., Ogée, J., Polcher, J., Friedlingstein, P., Ciais, P., Sitch, S., Prentice, I.C., 2005.
729   A dynamic global vegetation model for studies of the coupled atmosphere-biosphere system. Global Biogeochem. Cy. 19,
730   GB1015.

731 Li, C., 2007. Quantifying greenhouse gas emissions from soils: Scientific basis and modeling approach. Soil Sci. Plant Nutr. 53,
732   344–352.

733 Li, C., Aber, J., Stange, F., Butterbach-Bahl, K., Papen, H., 2000. A process-oriented model of N_2O and NO emissions from
734   forest soils: 1. Model development. J. Geophys. Res–Atmos. 105, 4369–4384.

735 Li, C., Frolking, S., Frolking, T.A., 1992. A Model of Nitrous Oxide Evolution From Soil Driven by Rainfall Events: 1. Model
736   Structure and Sensitivity. J. Geophys. Res. 97, 9759–9776.

737 Li, S., Zhang, W., Zheng, X., Li, Y., Han, S., Wang, R., Wang, K., Yao, Z., Liu, C., Zhang, C., 2022. Update of a
738   biogeochemical model with process-based algorithms to predict ammonia volatilization from fertilized cultivated uplands
739   and rice paddy fields. Biogeosciences 19, 3001–3019.

740 Li, S., Zheng, X., Zhang, W., Han, S., Deng, J., Wang, K., Wang, R., Yao, Z., and Liu, C., 2019. Modeling ammonia
741   volatilization following the application of synthetic fertilizers to cultivated uplands with calcareous soils using an
742   improved DNDC biogeochemistry model, Sci. Total Environ. 660, 931–946

743 Li, S., Zhu, B., Zheng, X., Hu, P., Han, S., Fan, J., Wang, T., Wang, R., Wang, K., Yao, Z., Liu, C., Zhang, W., Li, Y., 2023.
744   Enabling a process-oriented hydro-biogeochemical model to simulate soil erosion and nutrient losses. Biogeosciences
745   20, 3555−3572.

746 Li, X., 2019. Study on the relationship between vegetation productivity and water use in broadleaved-Korean pine forest zone
747   of Changbai Mountain of Jilin province, Northeast China. Dissertation, Beijing Forestry University.

748 Li, Y., Shen, J., Wang, Y., Gao, M., Liu, F., Zhou, P., Liu, X., Chen, D., Zou, G., Luo, Q., Ma, Q., 2017. CNMM: a
749   grid-based spatially-distributed catchment simulation model. China Science Press, Beijing (in Chinese).

750 Li, Y., Zhou, G., Zhang, D., Wenigmann, K.O., Otieno, D., Tenhunen, J., Zhang, Q., Yan, J., 2012. Quantification of
751   ecosystem carbon exchange characteristics in a dominant subtropical evergreen forest ecosystem. Asia-Pac. J. Atmos. Sci.
752   48, 1–10.

753 Li, Y., 2018. Spatiotemporal heterogeneity analysis of parameter sensitivity of ecological process model—the BIOME-BGC
754   model as an example. Dissertation, Northwest A & F University.

Liang, H., Hu, K., Batchelor, W.D., Qi, Z., Li, B., 2016. An integrated soil-crop system model for water and nitrogen management in North China. Sci. Rep. 6, 25755.

Liu, K., Ran, Q., Li, F., Shaheen, S.M., Wang, H., Rinklebe, J., Liu, C., Fang, L., 2022. Carbon-based strategy enables sustainable remediation of paddy soils in harmony with carbon neutrality. Carbon Res. 1, 12.

Liu, Q., 2018. Data assimilation study of Biome-BGC ecologyical process model and remote sensing observation LAI under three typical vegetation types. Dissertation, Northwest A & F University.

Lu, H., Li, S., Ma, M., Bastrikov, V., Chen, X., Ciais, P., Dai, Y., Ito, A., Ju, W., Lienert, S., Lombardozzi, D., Lu, X., Maignan, F., Nakhavali, M., Quine, T., Schindlbacher, A., Wang, J., Wang, Y., Wårlind, D., Zhang, S., Yuan, W., 2021. Comparing machine learning-derived global estimates of soil respiration and its components with those from terrestrial ecosystem models. Environ. Res. Lett. 16, 054048.

Ma, Q., Xiong, L., Li, Y., Li, S., Xu, C.Y., 2018. Partitioning multi-source uncertainties in simulating nitrogen loading in stream water using a coherent, stochastic framework: Application to a rice agricultural watershed in subtropical China. Sci. Total Environ. 618, 1298–1313.

Majkowski, J., Ridgeway, J.M., Miller, D.R., 1981. Multiplicative sensitivity analysis and its role in development of simualtion models. Ecol. Model. 12, 191–208.

Makela, A., Landsberg, J., Ek, A.R., Burk, T.E., Ter-Mikaelian, M., Ågren, G.I., Oliver, C.D., Puttonen, P., 2000. Process-based models for forest ecosystem management: current state of the art and challenges for practical implementation. Tree Physiol. 20, 289–298.

Mao, F., Li, P., Zhou, G., Du, H., Xu, X., Shi, Y., Mo, L., Zhou, Y., Tu, G., 2016. Development of the BIOME-BGC model for the simulation of managed Moso bamboo forest ecosystems. J. Environ. Manage. 172, 29–39.

Miyauchi, T., Machimura, T., Saito, M., 2019. Estimating carbon fixation of plant organs for afforestation monitoring using a process-based ecosystem model and ecophysiological parameter optimization. Ecol. Evol. 9, 8025–8041.

Moriasi, D., Arnold, J., Van Liew, M., Bingner, R., Harmel, R., Veith, T., 2007. Model evaluation guidelines for systematic quantification of accuracy in watershed simulation. T. Am. Soc. Agr. Biol. Eng. 50, 885–900.

Nash, J., Sutcliffe, J., 1970. River flow forecasting through conceptual models: part I- a discussion of principles. J. Hydrol. 10, 282–290.

Nobel, P.S., 1991. Phsiochemical and Environmental Plant Physiology. San Diego, CA, Academic Press.

Odongo, V.O., Onyando, J.O., Mutua, B.M., van Oel, P.R., Becht, R., 2013. Sensitivity analysis and calibration of the Modified Universal Soil Loss Equation (MUSLE) for the upper Malewa Catchment, Kenya. Int. J. Sediment Res. 28, 368–383.

Palosuo, T., Foereid, B., Svensson, M., Shurpali, N., Lehtonen, A., Herbst, M., Linkosalo, T., Ortiz, C., Rampazzo Todorovic, G., Marcinkonis, S., Li, C., Jandl, R., 2012. A multi-model comparison of soil carbon assessment of a coniferous forest stand. Environ. Modell. Softw. 35, 38–49.

Pianosi, F., Beven, K., Freer, J., Hall, J.W., Rougier, J., Stephenson, D.B., Wagener, T., 2016. Sensitivity analysis of environmental models: A systematic review with practical workflow. Environ. Modell. Softw. 79, 214–232.

Piao, S., Sitch, S., Ciais, P., Friedlingstein, P., Peylin, P., Wang, X., Ahlstrom, A., Anav, A., Canadell, J.G., Cong, N., Huntingford, C., Jung, M., Levis, S., Levy, P.E., Li, J., Lin, X., Lomas, M.R., Lu, M., Luo, Y., Ma, Y., Myneni, R.B.,

792   Poulter, B., Sun, Z., Wang, T., Viovy, N., Zaehle, S., Zeng, N., 2013. Evaluation of terrestrial carbon cycle models for
793   their response to climate variability and to CO2 trends. Global Chang Biol. 19, 2117–2132.

794   Potter, C.S., Randerson, J.T., Field, C.B., Matson, P.A., Vitousek, P.M., Mooney, H.A., 1993. Terrestrial ecosystem
795   production: a process model based on global satellite and surface data. Global Biogeochem. Cy. 74, 811–841.

796   Raczka, B.M., Davis, K.J., Huntzinger, D., Neilson, R.P., Poulter, B., Richardson, A.D., Xiao, J., Baker, I., Ciais, P., Keenan,
797   T.F., Law, B., Post, W.M., Ricciuto, D., Schaefer, K., Tian, H., Tomelleri, E., Verbeeck, H., Viovy, N., 2013. Evaluation
798   of continental carbon cycle simulations with North American flux tower observations. Ecol. Monogr. 83, 531–556.

799   Raj, R., Hamm, N.A.S., van der Tol, C., Stein, A., 2014. Variance-based sensitivity analysis of BIOME-BGC for gross and net
800   primary production. Ecol. Model. 292, 26–36.

801   Reich, P.B., Ellsworth, D.S., Walters, M.B., Vose, J.M., Gresham, C., Volin, J.C., Bowman, W.D., 1999. Generality of leaf
802   trait relationships: A test across six biomes. Ecology 80, 1955–1969.

803   Ren, H., Zhang, L., Yan, M., Tian, X., Zheng, X., 2022. Sensitivity analysis of Biome-BGCMuSo for gross and net primary
804   productivity of typical forests in China. For. Ecosyst. 9, 100011.

805   Running, S.W., Nemani, R.R., Heinsch, F.A., Zhao, M., Reeves, M., Hashimoto, H., 2004. A continuous satellite-derived
806   measure of global terrestrial primary production. BioScience 54, 547–560.

807   Ryan, M.G., 1991. Effects of Climate Change on Plant Respiration. Ecol. Appl. 1, 157–167.

808   Saltelli, A., Chan, K., Scott, E.M.(Eds.), 2000. SensitivityAnalysis. Wiley, Chichester.

809   Saltelli, A., Ratto, M., Andres, T., Campolongo, F., Cariboni, J., Gatelli, D., Saisana, M., Tarantola, S., 2008. Global
810   Sensitivity Analysis: The Primer. John Wiley & Sons, Ltd., Chichester.

811   Sato, H., Kumagai, T.o., Takahashi, A., Katul, G.G., 2015. Effects of different representations of stomatal conductance
812   response to humidity across the African continent under warmer CO_2-enriched climate conditions. J. Geophys. Res–
813   Biogeo. 120, 979–988.

814   Schulze, E.D., Luyssaert, S., Ciais, P., Freibauer, A., Janssens, I.A., Soussana, J.F., Smith, P., Grace, J., Levin, I.,
815   Thiruchittampalam, B., Heimann, M., Dolman, A.J., Valentini, R., Bousquet, P., Peylin, P., Peters, W., Rödenbeck, C.,
816   Etiope, G., Vuichard, N., Wattenbach, M., Nabuurs, G.J., Poussi, Z., Nieschulze, J., Gash, J.H., Team, C., 2009.
817   Importance of methane and nitrous oxide for Europe's terrestrial greenhouse-gas balance. Nat. Geosic. 2, 842–850.

818   Seidl, R., Thom, D., Kautz, M., Martin-Benito, D., Peltoniemi, M., Vacchiano, G., Wild, J., Ascoli, D., Petr, M., Honkaniemi,
819   J., Lexer, M.J., Trotsiuk, V., Mairota, P., Svoboda, M., Fabrika, M., Nagel, T.A., Reyer, C.P.O., 2017. Forest disturbances
820   under climate change. Nat. Clim. Change 7, 395–402.

821   Sitch, S., Smith, B., Prentice, I.C., Arneth, A., Bondeau, A., Cramer, W., Kaplan, J.O., Levis, S., Lucht, W., Sykes, M.T.,
822   Thonicke, K., Venevsky, S., 2003. Evaluation of ecosystem dynamics, plant geography and terrestrial carbon cycling in
823   the LPJ dynamic global vegetation model. Global Change Biol. 9, 161–185.

824   Srinet, R., Nandy, S., Patel, N.R., Padalia, H., Watham, T., Singh, S.K., Chauhan, P., 2023. Simulation of forest carbon fluxes
825   by integrating remote sensing data into biome-BGC model. Ecol. Model. 475, 110185.

826   Stitt, M., Schulze, D., 1994. Does Rubisco control the rate of photosynthesis and plant growth? An exercise in molecular
827   ecophysiology. Plant Cell Environ. 17, 465–487.

828 Tatarinov, F.A., Cienciala, E., 2006. Application of BIOME-BGC model to managed forests. Forest Ecol. Manag. 237, 267–
829   279.

830 Thomas, R.Q., Bonan, G.B., Goodale, C.L., 2013. Insights into mechanisms governing forest carbon response to nitrogen
831   deposition: a model–data comparison using observed responses to nitrogen addition. Biogeosciences 10, 3869–3887.

832 Thornton, P., Law, B., Gholz, H.L., Clark, K.L., Falge, E., Ellsworth, D., Goldstein, A., Monson, R., Hollinger, D., Falk, M.,
833   Chen, J., Sparks, J., 2002. Modeling and measuring the effects of disturbance history and climate on carbon and water
834   budgets in evergreen needleleaf forests. Agr. Forest Meteorol. 113, 185–222.

835 Thornton, P.E., Lamarque, J.-F., Rosenbloom, N.A., Mahowald, N.M., 2007. Influence of carbon-nitrogen cycle coupling on
836   land model response to CO_2 fertilization and climate variability. Global Biogeochem. Cy. 21, GB4018.

837 Tian, H., Liu, M., Zhang, C., Ren, W., Chen, G., Xu, X., Lu, C., 2005. DLEM—The Dynamic Land Ecosystem Model, User
838   Manual, The EDGE Laboratory, Auburn University, AL, USA.

839 Tian, H., Liu, M., Zhang, C., Ren, W., Xu, X., Cheng, G., Lv, C., Tao, B., 2010. The Dynamic Land Ecosystem Model (DLEM)
840   for Simulating Terrestrial Processes and Interactions in the Context of Multifactor Global Change. Acta Geographica
841   Sinca 65, 1027–1047.

842 Wang, W., Ichii, K., Hashimoto, H., Michaelis, A.R., Thornton, P.E., Law, B.E., Nemani, R.R., 2009. A hierarchical analysis
843   of terrestrial ecosystem model Biome-BGC: Equilibrium analysis and model calibration. Ecol. Model. 220, 2009–2023.

844 Waring, H.R., Running, S.W., 1998. Forest Ecosystems. Analysis at Multiples Scales. 2nd ed. Academic Press, San Diego, p.
845   55.

846 Waring, R.H., Running, S.W., 2007. Forest Ecosystems: Analysis at Multiple Scales. Francisco, CA, Elsevier Academic Press.

847 Wen, X., Wang, H., Wang, J., Yu, G., Sun, X., 2010. Ecosystem carbon exchanges of a subtropical evergreen coniferous
848   plantation subjected to seasonal drought, 2003–2007. Biogeosciences 7, 357–369.

849 Wen, Y., 2019. Coupling of landscape pattern and water use efficiency based on Biome-BGC model. Dissertation, Beijing
850   Forestry University.

851 White, M.A., Thornton, P.E., Running, S.W., Nemani, R.R., 2000. Parameterization and sensitivity analysis of the
852   Biome-BGC terrestrial ecosystem model: net primary production controls. Earth Interact. 4, 1–85.

853 Wigmosta, M., Vail, L., Lettenmaier, D., 1994. A distributed hydrology-vegetation model for complex terrain. Water Resour.
854   Res. 30, 1665–1679.

855 Willmott, C., Matsuurra, K., 2005. Advantages of the mean aboslute error (MAE) over the root mean square error (RMSE) in
856   assessing average model performance. Clim. Res. 30, 79–82.

857 Wu, J., Guan, D., Wang, A., Yuan, F., Diao, H., Yu, G., Chen, Z., Zhang, L., 2021. A dataset of carbon and water flux
858   observation in a broad-leaved red pine forest in Changbai Mountain (2003–2010). China Sci. Data 6, 2020-2011-2006.

859 Wu, L., McGechan, M.B., McRoberts, N., Baddeley, J.A., Watson, C.A., 2007. SPACSYS: Integration of a 3D root
860   architecture component to carbon, nitrogen and water cycling—Model description. Ecol. Model. 200, 343–359.

861 Wu, Y., Liu, S., Qiu, L., Sun, Y., 2016. SWAT-DayCent coupler: An integration tool for simultaneous hydro-biogeochemical
862   modeling using SWAT and DayCent. Environ. Modell. Softw. 86, 81–90.

863 Yan, M., Tian, X., Li, Z., Chen, E., Wang, X., Han, Z., Sun, H., 2016. Simulation of Forest Carbon Fluxes Using Model
864   Incorporation and Data Assimilation. Remote Sens. 8, 567.

Yu, G., Zhang, L., Sun, X., Fu, Y., Wen, X., Wang, Q., Li, S., Ren, C., Song, X., Liu, Y, Han, S., Yan, J., 2008. Environmental controls over carbon exchange of three forest ecosystems in eastern China. Global Change Biol. 14, 2555–2571.

Yu, G., Zhu, X., Fu, Y., He, H., Wang, Q., Wen, X., Li, X., Zhang, L., Zhang, L., Su, W., Li, S., Sun, X., Zhang, Y., Zhang, J., Yan, J., Wang, H., Zhou, G., Jia, B., Xiang, W., Li, Y., Zhao, L., Wang, Y., Shi, P., Chen, S., Xin, X., Zhao, F., Wang, Y., Tong, C., 2013. Spatial patterns and climate drivers of carbon fluxes in terrestrial ecosystems of China. Global Change Biol 19, 798–810.

Yuan, W., Cai, W., Xia, J., Chen, J., Liu, S., Dong, W., Merbold, L., Law, B., Arain, A., Beringer, J., Bernhofer, C., Black, A., Blanken, P.D., Cescatti, A., Chen, Y., Francois, L., Gianelle, D., Janssens, I.A., Jung, M., Kato, T., Kiely, G., Liu, D., Marcolla, B., Montagnani, L., Raschi, A., Roupsard, O., Varlagin, A., Wohlfahrt, G., 2014. Global comparison of light use efficiency models for simulating terrestrial vegetation gross primary production based on the LaThuile database. Agr. Forest Meteorol. 192–193, 108–120.

Zeng, H., Liu, Q., Feng, Z., Wang, X., Ma, Z., 2008. GPP and NPP study of *Pinus elliottii* forest in red soil hilly region based on BIOME-BGC model. Acta Ecol.Sinica 28, 5314–5321.

Zhang, L., Luo, Y., Liu, M., Chen, Z., Su, W., He, H., Zhu, Z., Sun, X., Wang, Y., Zhou, G., Zhao, X., Han, S., Ouyang, Z., Zhang, X., Zhang, Y., Liu, Q., Hao, Y., Yan, J., Zhang, D., Li, Y., Wang, A., Wu, J., Li, F., Zhao, F., Shi, P., Zhang, Y., He, Y., Lin, L., Song, Q., Wang, H., Liu, Y., Yu, G., 2019a. Carbon and water fluxes observed by the Chinese Flux Observation and Research Network (2003–2005). China Sci. Data 4, 2018-2012-2029.

Zhang, W., Li, S., Han, S., Zheng, X., Xie, H., Lu, C., Sui, Y., Wang, R., Liu, C., Yao, Z., Li, T., 2021a. Less intensive nitrate leaching from Phaeozems cultivated with maize generally occurs in northeastern China. Agr. Ecosyst. Environ. 310, 107303.

Zhang, W., Li, Y., Li, S., Zheng, X. 2024. The CNMM-DNDC V6.0 with the updates for simulating dynamical forest-atmosphere exchanges of carbon and evapotranspiration. Zenodo. https://doi.org/10.5281/zenodo.13363688.

Zhang, W., Li, Y., Zhu, B., Zheng, X., Liu, C., Tang, J., Su, F., Zhang, C., Ju, X., Deng, J., 2018. A process-oriented hydro-biogeochemical model enabling simulation of gaseous carbon and nitrogen emissions and hydrologic nitrogen losses from a subtropical catchment. Sci. Total Environ. 616–617, 305–317.

Zhang, W., Liu, C., Zheng, X., Wang, K., Cui, F., Wang, R., Li, S., Yao, Z., Zhu, J., 2019b. Using a modified DNDC biogeochemical model to optimize field management of a multi-crop (cotton, wheat, and maize) system: a site-scale case study in northern China. Biogeosciences 16, 2905–2922.

Zhang, W., Liu, C., Zheng, X., Zhou, Z., Cui, F., Zhu, B., Haas, E., Klatt, S., Butterbach-Bahl, K., Kiese, R., 2015. Comparison of the DNDC, LandscapeDNDC and IAP-N-GAS models for simulating nitrous oxide and nitric oxide emissions from the winter wheat–summer maize rotation system. Agr. Syst. 140, 1–10.

Zhang, W., Yao, Z., Li, S., Zheng, X., Zhang, H., Ma, L., Wang, K., Wang, R., Liu, C., Han, S., Deng, J., Li, Y., 2021b. An improved process-oriented hydro-biogeochemical model for simulating dynamic fluxes of methane and nitrous oxide in alpine ecosystems with seasonally frozen soils. Biogeosciences 18, 4211–4225.

Zhang, W., Yao, Z., Zheng, X., Liu, C., Wang, R., Wang, K., Li, S., Han, S., Zuo, Q., Shi, J., 2020. Effects of fertilization and stand age on N_2O and NO emissions from tea plantations: a site-scale study in a subtropical region using a modified biogeochemical model. Atmos. Chem. and Phys. 20, 6903–6919.

902 Zhang, Y., Li, C., Trettin, C.C., Li, H., Sun, G., 2002. An integrated model of soil, hydrology, and vegetation for carbon
903   dynamics in wetland ecosystems. Global Biogeochem. Cy. 16, 1061.
904 Zhou, G., Peng, C., Li, Y., Liu, S., Zhang, Q., Tang, X., Liu, J., Yan, J., Zhang, D., Chu, G., 2013. A climate change-induced
905   threat to the ecological resilience of a subtropical monsoon evergreen broad-leaved forest in Southern China. Global
906   Change Biol 19, 1197–1210.

Geoscientific
Model Development
Discussions

Open Access

EGU

Table 1 Statistics reflecting performances of original and updated CNMM-DNDC in simulating daily carbon fluxes of gross primary productivity (GPP) and ecosystem respiration (ER) three forest sites.

Item	Site	n[a]	NRMSE		NSE		Slope		R^{2}[d]	
			Ori[b]	Mod[c]	Ori	Mod	Ori	Mod	Ori	Mod
Daily GPP	CBM$_{cal}$	1826	0.94	**0.35**	0.19	**0.89**	0.77	**0.94**	0.29	**0.90**
	CBM$_{val}$	1096	1.21	**0.41**	-0.25	**0.85**	0.60	**0.93**	0.20	**0.86**
	QYZ$_{cal}$	1826	0.51	**0.35**	0.02	**0.55**	0.82	**0.85**	0.20	**0.68**
	QYZ$_{val}$	1096	0.47	**0.33**	0.18	**0.59**	0.55	**0.88**	0.65	**0.67**
	DHM$_{cal}$	1826	0.64	**0.35**	**-1.57**	**0.16**	0.75	**0.92**	-	**0.21**
	DHM$_{val}$	1096	0.64	**0.38**	**-1.68**	**0.08**	0.73	**0.89**	-	**0.18**
	All$_{cal}$	5478	0.71	**0.35**	0.03	**0.76**	0.79	**0.90**	0.19	**0.79**
	All$_{val}$	3288	0.80	**0.37**	-0.22	**0.74**	0.71	**0.90**	0.11	**0.79**
Daily ER	CBM$_{cal}$	1826	0.69	**0.21**	0.25	**0.93**	0.83	**1.00**	0.33	**0.93**
	CBM$_{val}$	1096	0.94	**0.27**	-0.35	**0.89**	0.65	**1.08**	0.11	**0.90**
	QYZ$_{cal}$	1826	0.57	**0.26**	-0.53	**0.68**	0.83	**0.93**	-	**0.71**
	QYZ$_{val}$	1096	0.52	**0.21**	-0.41	**0.77**	0.45	**1.05**	0.40	**0.78**
	DHM$_{cal}$	1826	0.59	**0.24**	-1.32	**0.62**	0.73	**0.92**	-	**0.68**
	DHM$_{val}$	1096	0.51	**0.18**	-0.76	**0.78**	0.83	**1.00**	-	**0.78**
	All$_{cal}$	5478	0.64	**0.24**	0.03	**0.87**	0.81	**0.96**	0.17	**0.87**
	All$_{val}$	3288	0.69	**0.23**	-0.34	**0.85**	0.77	**1.05**	-	**0.86**
Daily NEE	CBM$_{cal}$	1826	3.79	**2.85**	0.02	**0.45**	0.60	**0.71**	0.15	**0.55**
	CBM$_{val}$	1096	3.55	**2.47**	-0.09	**0.47**	0.50	**0.69**	0.17	**0.61**
	QYZ$_{cal}$	1826	0.95	**1.17**	0.35	**0.00**	0.83	**0.64**	0.40	**0.32**
	QYZ$_{val}$	1096	1.28	**1.59**	0.29	**-0.09**	0.75	**0.57**	0.41	**0.34**
	DHM$_{cal}$	1826	1.13	**1.05**	-0.20	**-0.04**	0.80	**0.87**	-	**-**
	DHM$_{val}$	1096	1.83	**1.71**	-0.28	**-0.11**	0.55	**0.63**	-	**0.02**
	All$_{cal}$	5478	1.49	**1.39**	0.13	**0.24**	0.75	**0.70**	0.19	**0.38**
	All$_{val}$	3288	2.04	**1.84**	-0.01	**0.18**	0.60	**0.63**	0.19	**0.40**
Daily ET	CBM$_{cal}$	1826	0.48	**0.46**	0.74	**0.76**	1.09	**1.07**	0.76	**0.77**
	CBM$_{val}$	1096	0.47	**0.42**	0.76	**0.81**	0.97	**0.99**	0.76	**0.81**
	QYZ$_{cal}$	1826	0.83	**0.40**	-0.31	**0.70**	0.69	**0.98**	0.08	**0.70**
	QYZ$_{val}$	1096	0.70	**0.32**	0.00	**0.80**	0.50	**1.07**	0.41	**0.81**
	DHM$_{cal}$	1826	0.72	**0.42**	-0.57	**0.47**	0.73	**0.96**	-	**0.47**
	DHM$_{val}$	1096	0.68	**0.35**	-0.55	**0.59**	0.72	**0.93**	-	**0.62**
	All$_{cal}$	5478	0.74	**0.43**	0.03	**0.68**	0.76	**0.99**	0.22	**0.68**
	All$_{val}$	3288	0.68	**0.35**	0.18	**0.78**	0.96	**1.00**	0.48	**0.78**

CBM, QYZ and DHM represent the forest site names of Changbai Mountains, Qianyanzhou and Dinghu Mountains, respectively. The subscripts of cal and val indicate the results during the periods of calibration (in 2003–2007) and validation (in 2008–2010), respectively, for all the sites. n denotes the number of daily or annual observations. Ori and Mod columns contain the statistics on simulations of the original and updated CNMM-DNDC, respectively. NRMSE, NSE, Slope and R^2 column contain statistics of normalized root mean square error, Nash-Sutcliffe efficiency, and the slope and determination coefficient of zero-intercept linear regression.

916 Table 2 Statistics reflecting performances of original and updated CNMM-DNDC in simulating annually cumulated carbon
917 fluxes of gross primary productivity (GPP) and ecosystem respiration (ER) across all three forest sites.
918

Item	Site	n	NRMSE		NSE		Slope		R^2	
			Ori	Mod	Ori	Mod	Ori	Mod	Ori	Mod
Annual GPP	All$_{cal}$	15	0.10	**0.07**	0.04	**0.61**	1.08	**0.98**	0.51	**0.64**
	All$_{val}$	9	0.13	**0.06**	0.04	**0.79**	0.99	**0.98**	0.04	**0.80**
Annual ER	All$_{cal}$	15	0.13	**0.10**	0.40	**0.67**	1.08	**0.98**	0.60	**0.68**
	All$_{val}$	9	0.19	**0.12**	-0.69	**0.33**	1.07	**1.08**	-	**0.62**
Annual NEE	All$_{cal}$	15	0.23	**0.26**	0.66	**0.55**	1.06	**0.98**	0.69	**0.55**
	All$_{val}$	9	0.48	**0.51**	-0.71	**-0.96**	0.74	**0.71**	0.19	**0.28**
Annual ET	All$_{cal}$	15	0.17	**0.13**	0.29	**0.61**	0.96	**0.99**	0.34	**0.61**
	All$_{val}$	9	0.07	**0.08**	0.89	**0.88**	0.99	**0.98**	0.89	**0.89**

919 Meanings of all abbreviations and subscripts, as well as year periods for the calibrations and validations are found in the
920 footnotes of Table 1.

Geoscientific
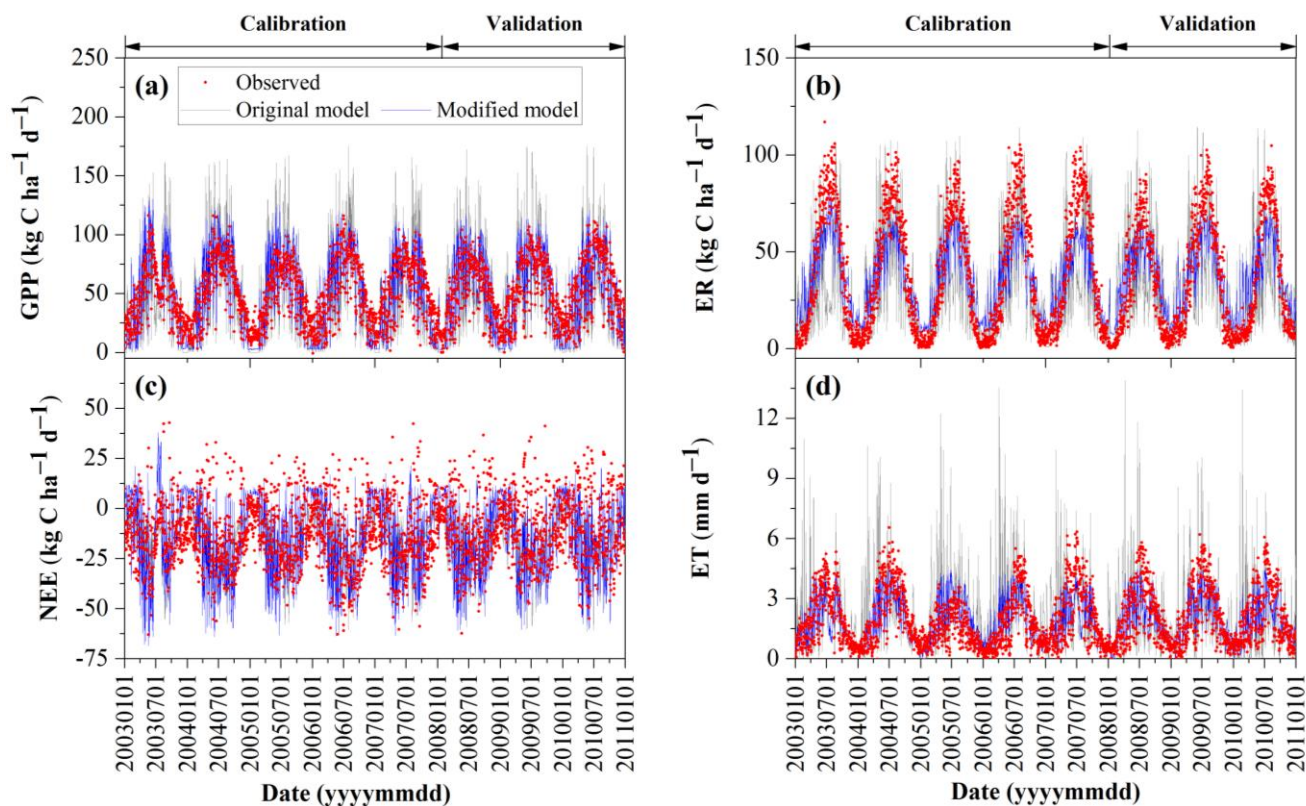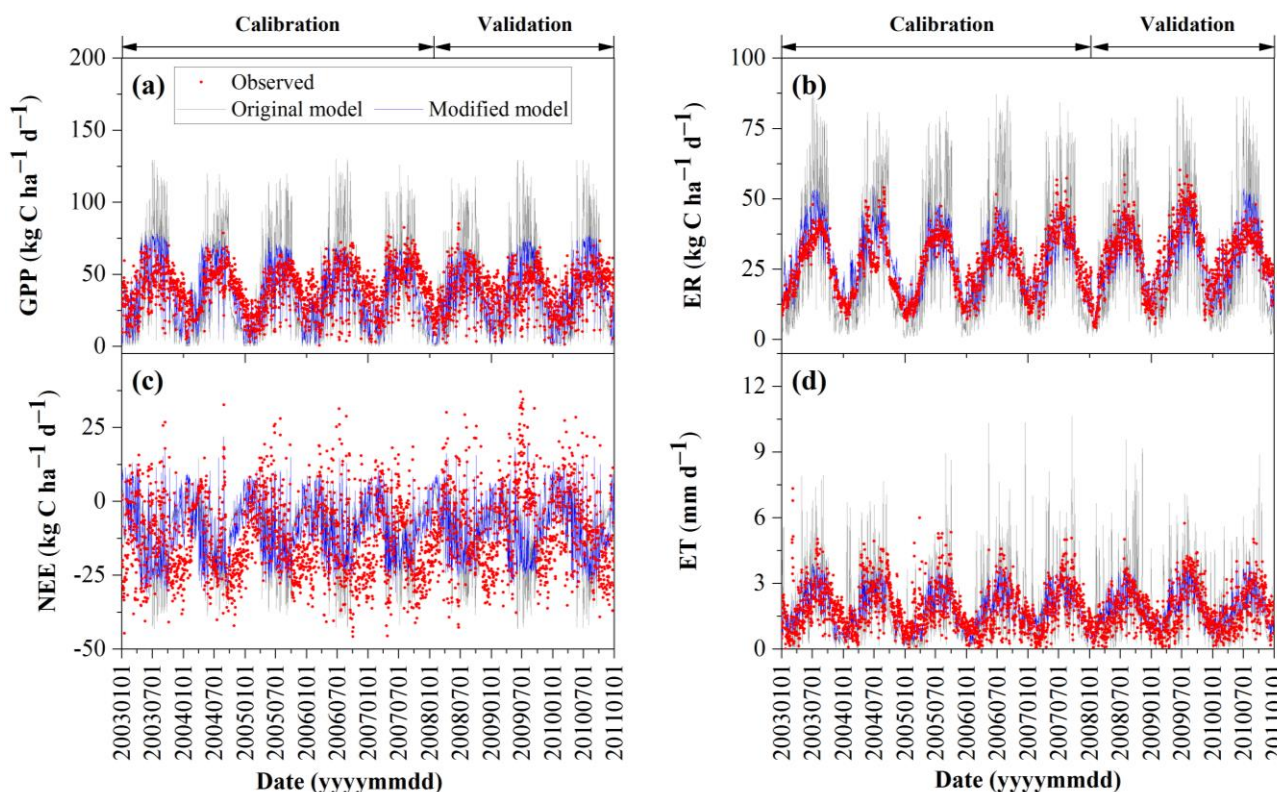Model Development
Discussions
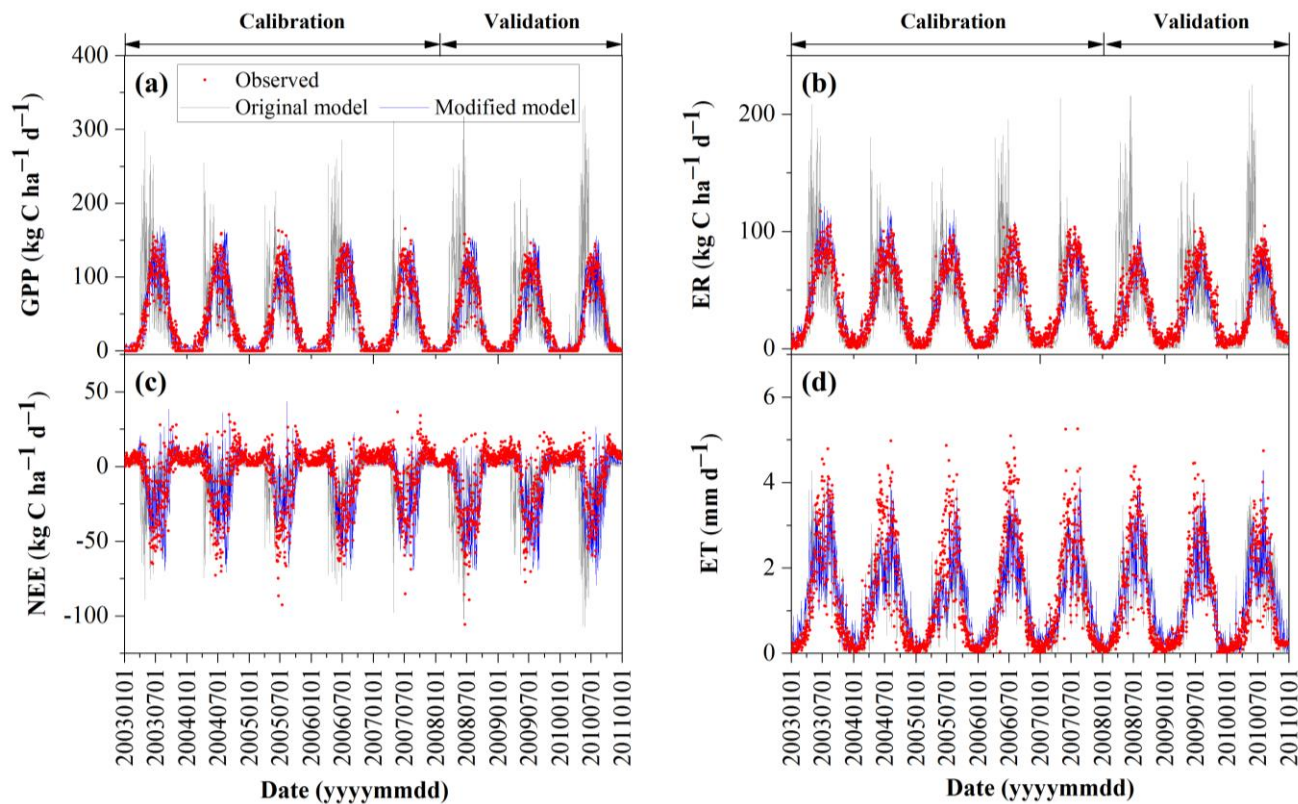
Figures

Figure: 1 Observations and simulations of original and modified CNMM-DNDC model on daily carbon fluxes of gross primary productivity (GPP), ecosystem respiration (ER) and net ecosystem-atmosphere exchange of carbon dioxide (NEE) and on daily water vapour fluxes of evapotranspiration (ET) from temperate mixed forest of evergreen needle leaf and deciduous broad leaf trees at the Changbai Mountain (CBM) site. The legends in panel a apply for other panels.

928

Figure 2: Observations and simulations of original and modified CNMM-DNDC model on daily carbon fluxes of gross primary productivity (GPP), ecosystem respiration (ER) and net ecosystem-atmosphere exchange of carbon dioxide (NEE) and on daily water vapour fluxes of evapotranspiration (ET) from subtropical evergreen needle leaf forest at the Qianyanzhou (QYZ) site. The legends in panel a apply for all other panels.
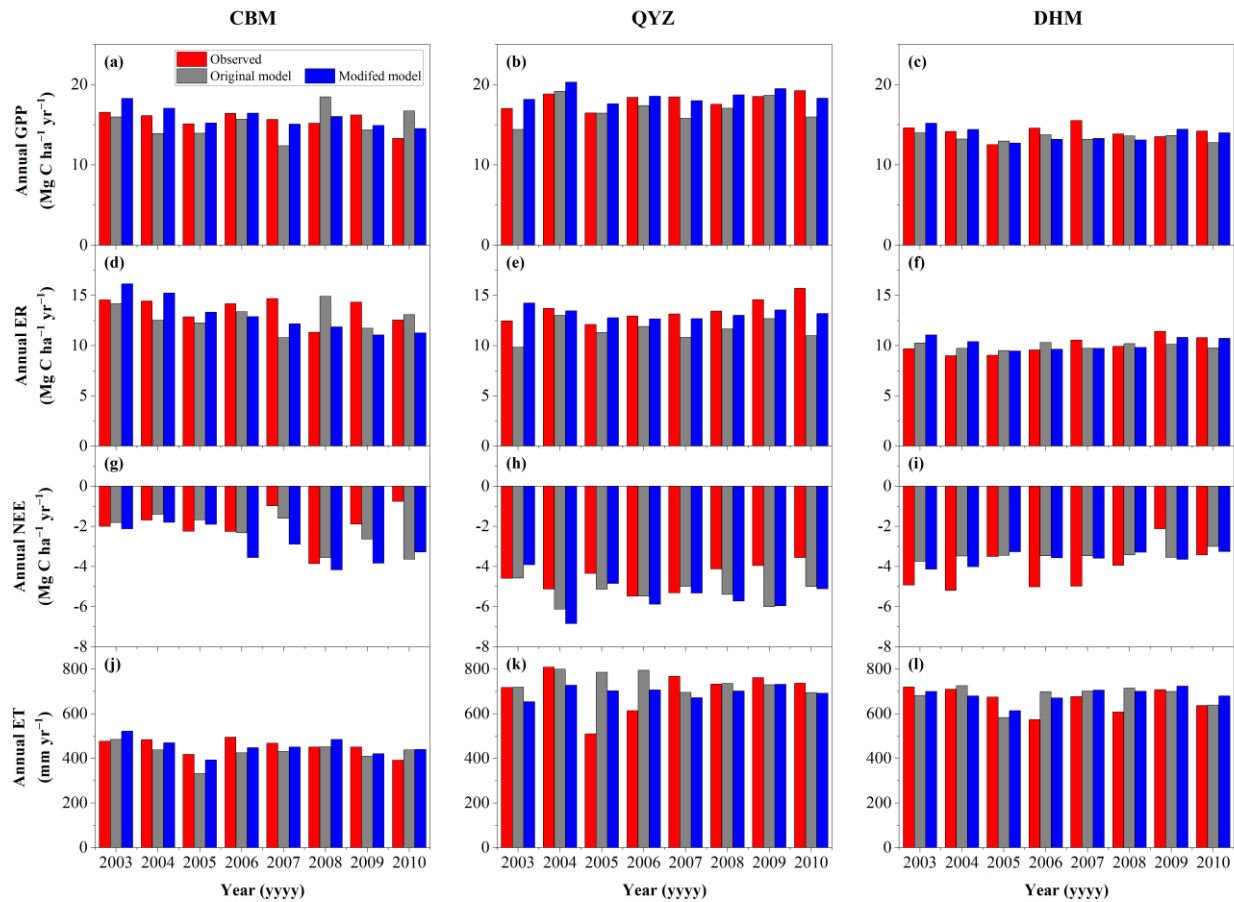
Figure 3: Observations and simulations of original and modified CNMM-DNDC model on daily carbon fluxes of gross primary productivity (GPP), ecosystem respiration (ER) and net ecosystem–atmosphere exchange of carbon dioxide (NEE) and on daily water vapour fluxes of evapotranspiration (ET) from subtropical mixing forest of evergreen needle and evergreen broad leaf trees at the Dinghu Mountains (DHM) site. The legends in panel a apply for all other panels.
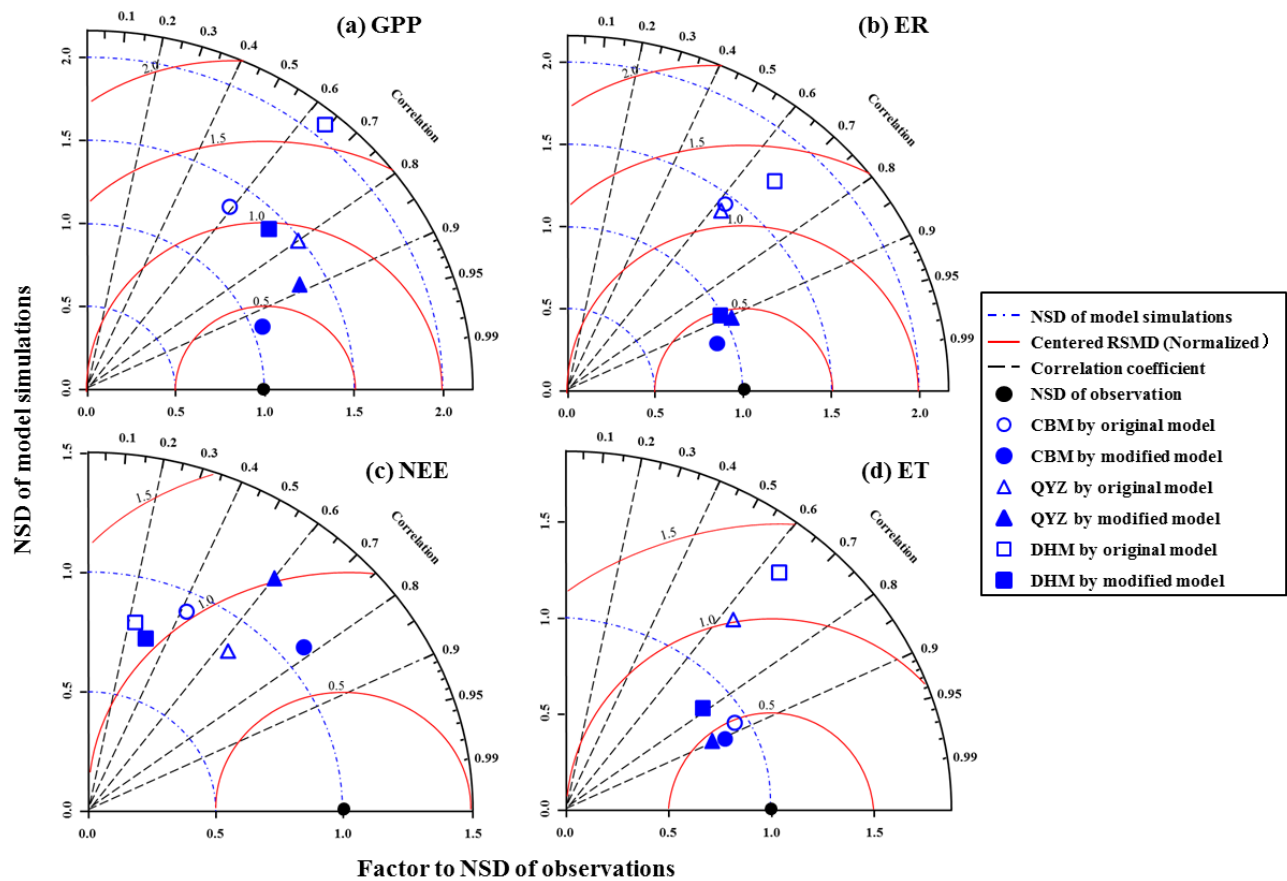
Figure: 4 Performance of original (empty grey symbols) and modified (solid blue symbols) model versions compared to observations (black solid points) at each forest site in validation years (2008–2010). Statistics shown in the Taylor diagrams are for daily simulated and observed carbon fluxes of gross primary productivity (GPP), ecosystem respiration (ER) and net ecosystem-atmosphere exchange of carbon dioxide (NEE), and water vapour fluxes of evapotranspiration (ET). The full site names of CBM, QYZ, and DHM are referred to the footnotes of Table 1.

944

Figure: 5 Observed and simulated annual carbon fluxes of gross primary productivity (GPP), ecosystem respiration (ER) and net ecosystem-atmosphere exchange of carbon dioxide (NEE) and water vapour fluxes of evapotranspiration (ET) at three forest sites. The full site names of CBM, QYZ and DHM are referred to the footnotes of Table 1. The legends in panel a apply for all other panels. The simulations were provided by the original and modified CNMM-DNDC model.

949
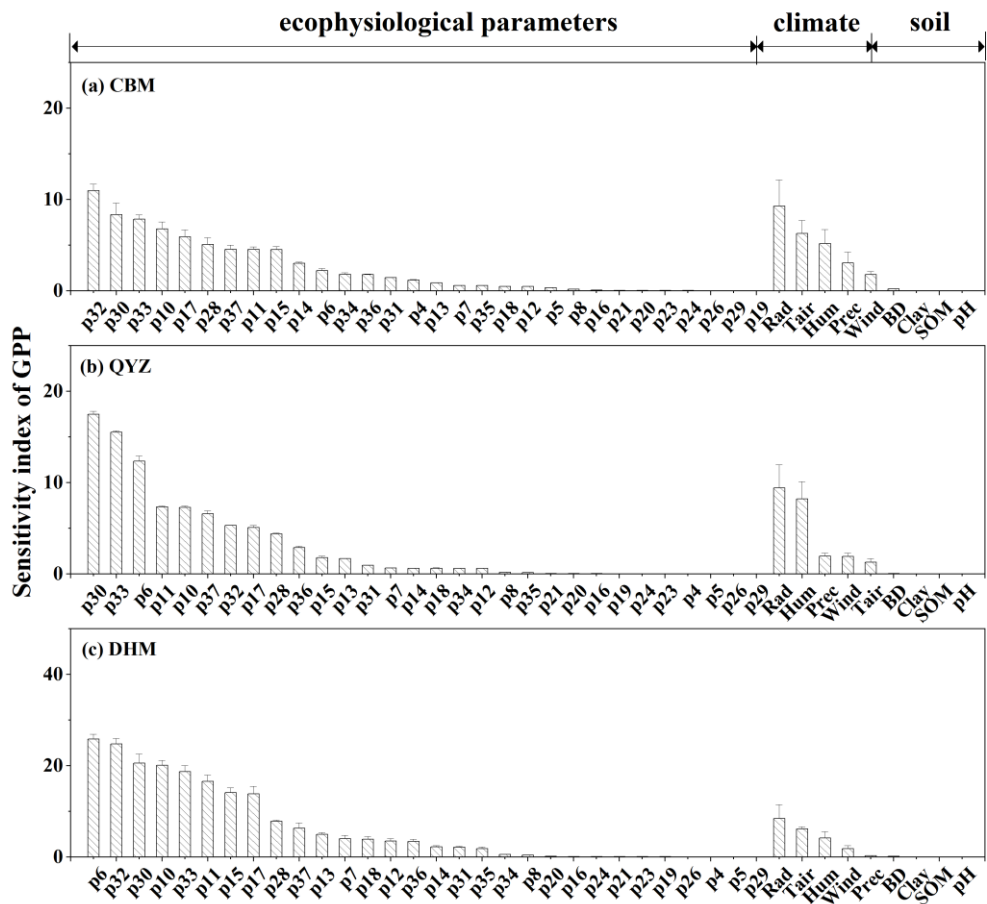
Figure: 6 Sensitivity indexes of modified CNMM-DNDC simulations on gross primary productivity responding to alternations in individual eco-physiological parameters and model inputs of meteorological variables and soil properties at each site. An index is given as the mean (a wide bar) and standard deviation (an error bar) of three indexes, each resulted from the simulations for one year. The parameter name and value for each parameter are referred to Table S2.
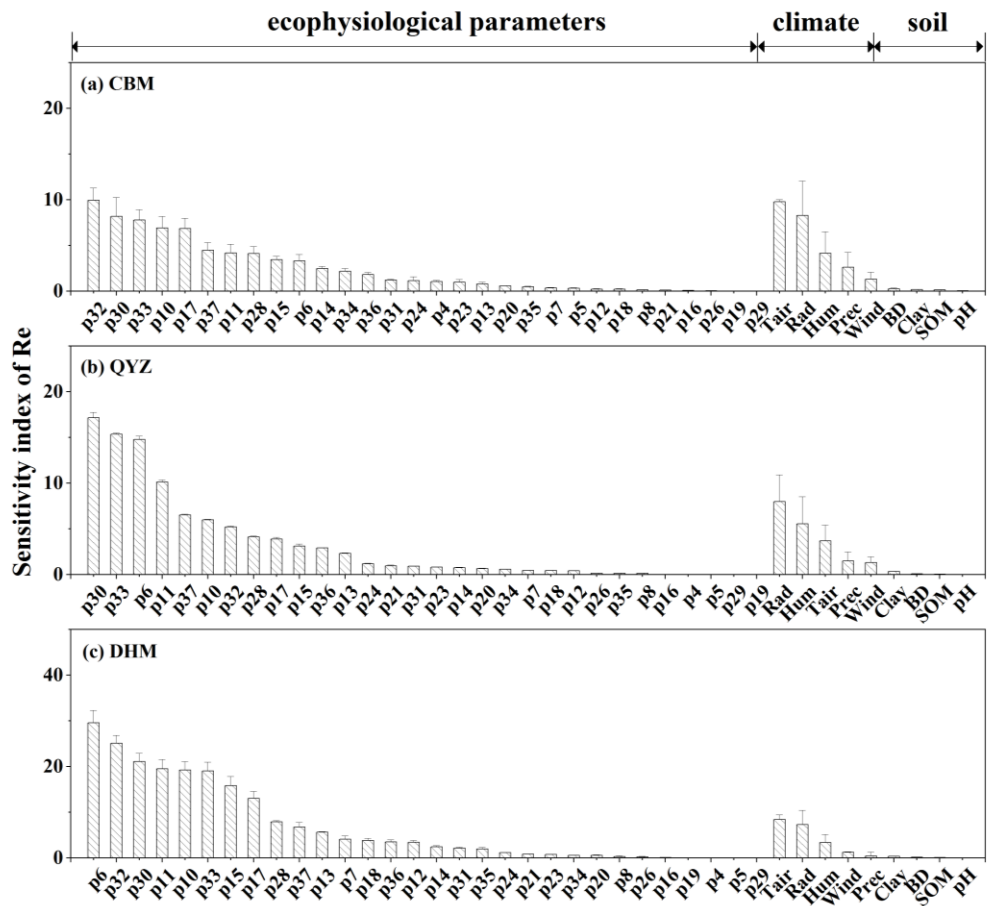
954

Figure: 7 Sensitivity indexes of modified CNMM-DNDC simulations on ecosystem respiration responding to alternations in individual eco-physiological parameters and model inputs of meteorological variables and soil properties at each site. An index is given as the mean (a wide bar) and standard deviation (an error bar) of three indexes, each resulted from the simulations for one year. The parameter name and value for each parameter are referred to Table S2.